Water Resources and Industry 31 (2024) 100251

Contents lists available at ScienceDirect

Water Resources and Industry

journal homepage: www.elsevier.com/locate/wri

Catalysts for advanced oxidation processes: Deep eutectic solvents-assisted synthesis – A review

Amir Mohammad Sheikh Asadi [a,b], Łukasz Cichocki [b], Ali Atamaleki [c], Marjan Hashemi [d], Holger Lutze [a,**], Muhammad Imran [e], Lingshuai Kong [f], Chongqing Wang [g], Grzegorz Boczkaj [b,h,*]

[a] Chair of Environmental Analytics and Pollutants, Institute IWAR, Technical University of Darmstadt, Darmstadt, Germany
[b] Department of Sanitary Engineering, Faculty of Civil and Environmental Engineering, Gdansk University of Technology, Gdansk, Poland
[c] Department of Environmental Health Engineering, School of Public Health, North Khorasan University of Medical Sciences, Bojnurd, Iran
[d] Environmental and Occupational Hazards Control Research Center, Research Institute for Health Sciences and Environment, Shahid Beheshti University of Medical Sciences, Tehran, Iran
[e] Centre for Inorganic Chemistry, School of Chemistry, University of the Punjab Lahore, 54000, Pakistan
[f] Institute of Eco-Environmental Forensics, School of Environmental Science and Engineering, Shandong University, Qingdao, 266237, China
[g] School of Chemical Engineering, Zhengzhou University, Zhengzhou, 450001, China
[h] EkoTech Center, Gdańsk University of Technology, G. Narutowicza St. 11/12, Gdansk, 80-233, Poland

ARTICLE INFO

Keywords:
Wastewater treatment
Radical reactions
Functional materials
Green synthesis
Green chemistry
Pharmaceuticals

ABSTRACT

New catalyst synthesis techniques, including green materials, are extensively studied for heterogeneous photocatalytic advanced oxidation processes (AOPs) on spotlight of sustainable development. Deep eutectic solvents (DESs) started to be used in this field as environmentally friendly alternative to ionic liquids (ILs).

During the catalyst synthesis, DESs can act as stabilizers, capping agents, structure directing agents, templates, hydrolyzing agents, etching agents, intercalators, and latent supramolecular catalysts. Importantly, DESs have exhibited the ability to significantly influence catalyst morphology, functionalization and photocatalytic properties (confirmed both for classic UV lamps and light emitting diode (LED)), including band-gap modification.

DESs positive effect was proved for a variety of materials, including metal oxides, metalorganic (MO) complexes and doped materials, MXene (MAX phase etching in DES environment), inorganic-organic hybrids, carbo-catalysts. Substantial enhancements were obtained for modification of photocatalytic materials like TiO_2, ZnO, MnO_2, iron oxides, ceria oxides, CdS, bismuth based photocatalysts and biochar modification. In this aspect, a particular role of DESs was confirmed for synthesis of nanomaterials in a form of nanoparticles, nanopowders or nanosheets.

Effectiveness was further increased by oxidants such as hydrogen peroxide, persulfates and Fenton process. Effective application of DES-modified catalysts was confirmed for degradation of dyes (Rhodamine B, Reactive orange 16, Safranine, Orange II, methylene blue), pharmaceuticals and antibiotics (Cefixime, Tetracycline, Oxytetracycline, Flumequine, Sulfamethaxazole), PFASs

* Corresponding author. Department of Sanitary Engineering, Faculty of Civil and Environmental Engineering, Gdansk University of Technology, Gdansk, Poland.

** Corresponding author. Chair of Environmental Analytics and Pollutants, Institute IWAR, Technical University of Darmstadt, Darmstadt, Germany.

E-mail addresses: holger.lutze@tu-darmstadt.de (H. Lutze), grzegorz.boczkaj@gmail.com, grzegorz.boczkaj@pg.edu.pl (G. Boczkaj).

https://doi.org/10.1016/j.wri.2024.100251
Received 4 December 2023; Received in revised form 2 February 2024; Accepted 27 February 2024
Available online 2 March 2024

(Perfluorooctanoic acid) and Cr(VI). This reveals high potential of DES based photocatalysts for environmental engineering and remediation.

There are still remaining a significant gaps in our understanding of the roles and impacts of DESs in AOPs. Furthermore, there is an absence of data regarding the recovery of DESs in the catalyst synthesis processes applied in AOPs. Addressing this aspects is vital for economic and environmentally friendly applications. As research progresses, it is essential to unravel the intricacies of DES-mediated catalyst synthesis and their broader consequences.

List of abbreviations

C	Carbon
CF_3SO_3H	Trifluoromethanesulfonic Acid
ChPh	Choline Phosphate
CTAB	Cetyltrimethylammonium Bromide
DEG	Diethylene Glycol
EG	Ethylene Glycol
GO	Graphene Oxide
HBF_4	Tetrafluoroboric Acid
HPF_6	Hexafluorophosphoric Acid
Hq	Hydroquinone
MCl	Metal Chloride
MO	Metal Oxide
mp	Melting point
MS	Metal Sulfide
NG	Neat Graphene
NP	Nanoparticle
PEG	Polyethylene Glycol
PTSA	p-toluene sulphonic acid
TBT	Titanium Butoxide

1. Introduction

This review presents a state-of-the-art on DESs applications for preparation of catalysts for AOPs. According to collected literature it relates to 2010–2024 period (Fig. 1).

A numerous of organic contaminants can be found in water bodies, it is caused by wastewater discharge into the environment [1]. Even after suitable operations and processes taking place in wastewater treatment plants, effluents disposed contain some pollutants – often persistent to degradation by biological treatment methods. As such pollutants can accumulate in the environment, they are of increasing public concerns due to the ecological and health issues. Therefore, substantial effective attempts have been made to overcome such dilemmas. Accordingly, advanced oxidation processes (AOPs) can be named one of the promising techniques to fulfill the water and wastewater treatment's needs. AOPs form reactive radical species, mainly hydroxyl radicals ($^{\cdot}OH$, $E^0 = 1.8–2.7$ V),

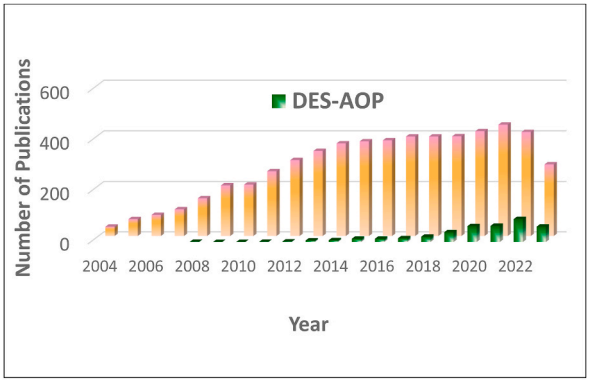

Fig. 1. Comparison of the number of publications on IL and DES-assisted catalysts applied in AOPs between 2004 and 2022.

while other radical based technologies are based on different reactive species such as sulfate radicals ($SO_4^{\cdot-}$, E^0 = 2.5–3.1 V) [2].

There are two types of AOPs: homogeneous and heterogeneous processes, which have indicated their superiority and advantages in the removal of organic pollutants from water and wastewater [3–5]. Accordingly, reaching the applicable, environmentally friendly, economical, and effective solid-phase catalysts have been turned out a hot topic in chemistry, engineering as well as material science [6–8].

New routes of catalysts synthesis, including green materials, are studied to obtain novel catalysts for heterogeneous AOPs but also to meet the requirements for sustainable applications. For instance, photocatalytic processes (PCPs) are vitally dependent on catalysts properties such as their morphology, surface area, aggregation, toxicity, chemical structure, and mechanical resistance which can dramatically increase or decrease their applicability for specific purpose [9,10].

In recent decade a high attention was made for ionic liquids (ILs) assisted synthesis of catalysts [11]. Several advantages relating to obtained size and structure of as synthesized catalysts were reported [12,13]. Disadvantages include limited solubility of metal cations in the solvent, limited pH during catalyst synthesis and limited metal loading (e.g. Co onto TiO_2) [14,15]. One of raising issues with ILs relates to their toxicity. Currently a new trend in catalysts synthesis is strongly observed. Popularity of applications based on deep eutectic solvents (DESs) usage reached also into this field. DESs firstly introduced by Abbott et al. [16,17] offers competitive properties to ILs, while toxicity of many compounds used to obtain DESs is minimized.

DESs are synthesized from at least two constituents, a hydrogen-bond donor (HBD) and a hydrogen-bond acceptor (HBA), that can form hydrogen bonds, allowing them that under particular molar ratios, the mixture has a melting point at a much lower temperature than that of each component [18]. Examples include choline chloride (malting point (mp) = 302 °C) mixture with malonic acid (mp = 133 °C) in molar ratio 1:1 to obtain DES (mp = 10 °C) [19] or betaine (mp = 310 °C) mixture with malic acid (mp = 130 °C) in molar ratio 1:1 to obtain DES (mp = 45 °C) [20]. In many cases DES melting point is much below the room temperature. Several controversial proposals have been recommended to clarify the creation process of DESs; however, cluster formation and the mechanical mixture are the most important assumptions for DES development [21]. According to A. P. Abbott et al. the HBD associates with the anion of the HBA and increases its effective size. As a result, the interaction with the cation is minimized, and the mixture's melting point is lowered [22].

As shown in Fig. 1., there was a noticeable increase in the publications of ILs-assisted synthesis of catalysts applying in AOPs. In other words, there were just three publications in 2004 while this number was reached over 100 publications by the end of 2021. While the first papers were regarding advanced oxidation applications of ILs-assisted catalysts, the DES was just discovered. After six years, Liu et al. brought the DESs-assisted catalysts to the attention, and since then, a growth of interest on DESs was observed in scientific publications. Despite this climb, the number of publications of DES-based materials is substantially lacking in comparison to ILs-based ones. This may be due to the fact that DESs are recently developed and need more time to be known in the scientific environment; however, by a simple search, we can find 6520 publications between 2004 and 2021, indicating that DESs have drawn attention. According to already confirmed advantages, probably DESs in short time will find comparable to ILs interest in catalysts synthesis.

As mentioned before, DESs show not only the advantages of ILs but also significant superiorities such as biodegradability and reasonable price. Nevertheless, there is a question that has to be answered; can this difference be related to the DES's effect on catalysts?

In this review, we aimed to concentrate on DES's effect on AOP's catalysts. To fulfill this aim, DESs roles in the catalytic degradation processes were discussed. The physicochemical properties of synthesized catalysts that are affected by the utilization of DESs through the synthesis process were discreetly deliberated. According to our knowledge this is a first review articles on this aspect of DESs application.

2. Application of DESs in green synthesis

Since the beginning of the 1990s, green chemistry has been introduced to attain sustainability at the molecular level. The discipline, which includes twelve principles, has been dramatically grown up in the past decades. Green synthesis is a subgroup of green chemistry, and its fundamentals are acquired from the twelve principles, addressing sustainability concerns that conventional synthesis methods were unable to meet [23].

DESs, as green materials, can play a significant role in the green scenario because, in many cases, they can follow the most of green chemistry principles. For example, by utilizing various DESs as the solvent and reducing agents simultaneously at ambient temperature. Aruchamy et al. proposed an energy-free, solvent/reactant-free, and ultra-fast approach (1 min) to synthesize a binary metal oxide (Mn_xO_y) [24]. In their proposed method, at least five principles relating to waste minimization have been targeted by employing the DESs, such as prevention or reducing, atomic economy, safer solvent/auxiliaries, mitigation of environmental pollution, and energy efficiency.

One of the advantages of DESs is their high mutual compatibility with numerous metal salts. Therefore, DESs are able to maximize the incorporation of metal salts employed in the synthesis into the final product, such as metal oxides. Accordingly, Hammond et al. prepared a biodegradable choline chloride: urea DES as the solvent with a considerable molar concentration of the Fe precursor (0.25 mol kg^{-1}) to maximize the atom efficiency of the process whilst reducing solvent needs, design for the degradation, prevention, and atomic economy. Furthermore, they have demonstrated that choline chloride: urea DES, employing such synthesis precursors, serves as a supramolecular catalyst and pre-structuring agent, providing a milder condition by getting the reactants together, following another green chemistry principle which is about design for energy efficiency [25]. In the point of green chemistry point of view, nonessential additives should be avoided — as much as possible — because such efforts demand extra reagents and can produce more

wastes. According to reducing derivatives, Datta et al. have proposed a DES-based solvothermal synthesis regarding a surfactant-free green procedure for generating 3D, 2D, and 1D nanostructured V_2O_5 [26].

Since environmental experts always attempt to stick to green scenarios, such facts demonstrate the high capacity of DES to address the sustainable synthesis procedures, especially for generating metal oxides (MOs), indicating propitious catalysts for AOPs.

3. DES-assisted synthesis of catalysts for advanced oxidation processes

There is a variety of catalysts that can be employed in AOPs. However, with a precise look at the DES-assisted synthesized catalysts, we can figure out that the most applied ones are metal oxides (Table 1). When metal ions and oxides shape coordination bonds, MOs are formed. Among the MOs, TiO_2 and ZnO were more deliberated due to yielding high energy states of electron and hole pairs [27–29]. Despite the TiO_2 and ZnO's advantages, namely acceptable catalytic performance, chemical resistance, significant market potential, and non-toxicity, these two most applicable MOs possess some issues such as wide bandgap, fast recombination of electron/holes, and rough recycling. Many attempts have been proposed to overcome the obstacles, including doping the catalyst by metal and non-metal additives, using dedicated support materials, and improving the chemical and physical properties by utilizing unique structures such as MXenes, the latest generation of two-dimensional transition metal nitrides or carbides. Other forms of MOs have also been synthesized by means of DESs, such as binary metal oxides (BMOs) or more complex MOs, which indicated higher catalytic performance for AOP purposes compared to solo metal-based MOs [30–32]. Moreover, metal sulfides and chlorides, organic and inorganic complexes, and biochar and other carbon-like materials were also employed; however, they were less investigated compared to other types of DES-assisted catalysts [2,33,34].

Herein, we discuss all the mentioned catalysts and the role of DES in their synthesis procedure. Also, the effect of DES in their structures and performance will be precisely deliberated.

4. Role of DES in catalysts synthesis

Most of the traditional organic solvents are hazardous, poisonous, and destructive to the environment. As a result, their use threatens human health and the ecosystem. Consideration of the properties of the solvent and all its risks is essential for long-term sustainable use. The use of DES as newly invented solvents for MO synthesis has been widely studied. It follows from the fact that DESs may indicate multiple roles, i.e., to be a precursor and reducing agent, produce high yield product, diminish unwilling productions, provide the considerable potential for one-pot (or fewer steps) synthesis procedure, and enhance product separation. These features allow DESs to nourish sustainable synthesis processes, not only in laboratories but also in the industry [62].

Karimi et al. utilized DESs in the all-in-one system to fulfill three functions -solvent, template, and precursor. Accordingly, amorphous hematite nanoparticles were achieved at 130 °C. Because of the remarkable ionic strength of ferric chloride-choline chloride DES, the inter-particle connections necessary for electrostatic stabilization were diminished. Furthermore, the DES's bulky shape supplied the steric repulsion needed to avert aggregation by chemisorption on the surface of nanomaterials [39]. In the other study conducted by the same group, calcium chloride-choline chloride DES was employed to synthesize Monetite nanoparticles. In the synthesized process, the development and stabilization of the $CaHPO_4$ were achieved because of neutral to slightly acidic conditions, which the DES as a solvent provided. Another critical duty of DES was to form –Ca– positions, whereby DES reacted with PO_4^{3-} to compose $Ca_3(PO_4)_2$ precipitates. They also reported that the reacting DES with PO_4^{3-} led to calcium deficiency in the DES, resulting in altered integration between unreacted calcium chloride hexahydrate and choline chloride. The last function of the employed DES was a template related to the high ion density and three dimensional structure of the DES, which controlled the particle growth [63]. Similarly, Xu et al. studied in details the DES role in the synthesis of $CdS@CeO_2$ composites for application in AOP. In their work, several functions for each component of PEGylated DES (PEG 200 (average molar mass: 200 g/mol): thiourea) were reported. For example, they revealed that beside obvious application of thiourea as a sulfur source, it also formed a relatively stable metal-thiourea intermediate state in the reaction mixture, which was advantageous for CdS formation. Moreover, PEG 200 affected the both morphology and band gap of synthesized catalysts [33].

The another role of DES is the functionalization of catalysts to enhance their efficiency in environmental pollution degradation processes. For instance, Taghavi et al. proposed a grafting process in DES in which a rigid covalent bonding between the surface atoms of solid materials, TiO_2–P25, and the polymer chain, 2,4-toluene diisocyanate (TDI), was formed (Scheme 1).

The highly reactive linker, TDI, was utilized to act as a bifunctional covalent linker to bridge Ti to DESs for enhancing the catalyst's recyclability and durability. The synthesized inorganic-organic complex has been utilized as a covalently grafted acidic DES to photo-oxidize benzyl alcohols under light emitting diode (LED) illumination. $ZnCl_2$ groups that were used in the DES could be responsible for the higher photocatalytic activity of the complex because of the provided Lewis acidic sites. Furthermore, zinc ions in the structure of bonded DES and nano-sized TiO2–P25 formed a heterojunction configuration and, consequently, varied the bandgap [59].

One of the initial features of a catalyst, driving catalytic effectiveness, are the surface properties. The nanoparticles comprise high surface energy; thus, they might be aggregated, resulting in reducing the active site of the catalyst [11]. Moreover, lowered-sized catalysts can provide more active zones [64]. Thus, several approaches, including template and structure-directing effects, have been introduced to enhance the surface features [65,66]. These terms may be employed interchangeably, although sometimes they reflect dissimilarity. Since DESs can be applied as a template, such as capping agent and stabilizer [35], and structure-directing agent [36,48], these terms should be accurately defined to find the exact role of DESs in the synthesis processes.

On the one hand, the template effect appears while the nucleation or the gelation process is occurring by which DESs arrange low-molecular materials around themselves and provide certain geometric topologies. This is due to the difference in intermolecular

interactions, directing the build of well-ordered products [40,67]. More specifically, the capping agent could assist in averting the nanostructures from growth, but the stabilizing agent would prevent their agglomeration [68]. On the other hand, the incorporation of DESs directs the crystallization of a unique framework style called the structure-directing effect. That is to say, in the absence of structure-directing agents, the same synthesis reactions yield different products [69]. Since these effects occur simultaneously, authors may highlight one of them; however, the mechanisms of these effects are instinctively different. For instance, surfactants or polymers, playing roles as capping agents, have been nominated as an encouraging solution by lessening the surface energy [70]. As previously stated, due to achieving the principles of green synthesis, studies attempted to substitute polymers and surfactants with DES. Accordingly, Sri. V et al. highlighted the usefulness of ChCl: sucrose-based DES, behaving as a stabilizer as well as a capping agent, for synthesizing amorphous Fe nanoparticles, possessing tunable physicochemical properties [35]. Aihindh et al. concentrated on the directing effect of DES on $BiVO_4$ nanoparticles and demonstrated that nano-catalysts with exposed facets displayed a remarkable catalytic effect for reduction of Cr (VI) [49].

A significant issue regarding the synthesis of MOs is their yield and stability, limiting their industrial uses. Therefore, in several studies, DESs were served as a stabilizer due to its attractive properties that can reasonably control not only the stability of MOs but also the yields of nanoparticles. For example, Iqbal et al. proposed a synthesis method in which cetyltrimethylammonium bromide (CTAB): acetic acid-based DES was added dropwise to the solution containing ammonium cerium (IV) nitrate, isopropyl alcohol, and ethylene glycol, whereby a high yield of CeO_2 and the highly stable nanoparticles were obtained. This is due to the use of DES, which provides stabilizing effect for achieving mono-dispersed and non-agglomerated particles [37]. Likewise, Cun et al. synthesized well-dispersed and long-term stabilized ZnO nanostructures through a DES-based ionothermal procedure. They reported that

Table 1
DES-assisted synthesized AOP's catalysts.

No	Catalyst name	Classification	DES	M ratio	DES Role in Synthesis process	Ref.
1	amorphous Fe NP	MO	ChCl:sucrose	2:1	stabilizing/capping agent	[35]
2	nanosized anatase titania	MO	ChCl:Hq	2:1	structure-directing/capping agent	[36]
3	ceria NP	MO	CTAB:acetic acid	1:6	stabilizing	[37]
4	ε-manganese dioxide (ε-MnO_2)	MO	ChCl:urea	1:2	solvent	[38]
5	α-Fe_2O_3 (hematite) nanoparticles.	MO	ChCl:ferric chloride	1:2	solvent/precursor (Fe source)/template	[39]
6	coral-like TiO_2 NP	MO	ChCl:PTSA	1:1	Template/hydrolyzing agent	[40]
7	Mn_2O_3 nanoparticles	MO	ChCl:EG	1:2	solvent	
8	ZnO NPs	MO	ChCl:DEG	1:2	Solvent/stabilizing	[41]
9	TiO_2 NPs	MO	ChCl:EG ChCl:urea	1:2	electrolyte	[42]
10	ZnO nanosheets	MO	ChCl:urea	1:2	solvent	[43]
11	ZnO	MO	ChCl:urea	1:2	solvent	[44]
12	cubic Iron oxide NP	MO	ChCl: citric acid	2:1	solvent	[45]
13	Fe_3O_4 magnetic NP	MO	ChCl:urea	1:2	solvent	[46]
14	AFe_2O_4 (A = Mg, Zn and Mn)	Complex MO	ChCl:malonic acid	1:1	solvent	[32]
15	Ti_3C_2/TiO_2–$NaBF_4$	Complex MO	ChCl:HPF_6 ChCl:HBF_4 ChCl:CF_3SO_3H	1:1 1:2 1:3	etching agent/intercalator	[47]
16	BOC/BVO/g-CN	Complex MO	ChCl: citric acid	1:1	latent supramolecular catalysts/structure directing	[48]
17	$BiVO_4$	Complex MO	ChCl:urea	1:2	latent supramolecular catalysts/structure directing	[49]
18	BiOCl/$BiVO_4$@AgNWs	Complex MO	ChCl:urea	1:2	solvent	[50]
19	$BiVO_4$ microtubes	Complex MO	ChCl:urea	1:2	solvent	[51, 52]
20	N/P co-doped TiO_2	MO-Doped	Chph:urea	1:2	electrolyte	[53]
21	*N*-doped Ceria NPs	MO-Doped	CTAB: acetic acid	1:1	precursor/solvent	[54]
22	Ni–TiO_2 Composite	MO-Doped	ChCl:EG	1:2	electrolyte	[55]
23	ZnOGO	MO-Support	ChCl:EG	1:2	solvent	[56]
24	ZnO/NG	MO-Support	ChCl:DEG	1:2	solvent	[57]
25	CdS@CeO_2	MS	PEG 200: thiourea	2:1	precursor (sulfur source)/stable metal-thiourea/ morphological regulator/band-gap regulator	[33]
26	Ag@AgCl	MCl	ChCl:urea	1:2	solvent/precursor (chlorine source)/ reductant	[58]
27	n-TiO_2-P25@TDI@DES	Inorganic-organic complex	urea: $ZnCl_2$	4:1	functional component	[59]
28	$\|C_{10}H_{10}N_2\|[GaF(C_2O_4)_2]$	Inorganic-organic complex	ChCl: Oxalic acid	1:2	precursor (oxalate source)	[60]
29	Ti/SnO_2eSb electrode	Electrode	ChCl:EG	1:2	electrolyte	[61]
30	nitrogen-doped biochar	Organic material	ChCl:urea	1:2	modifier/precursor (nitrogen source)	[34]

diethylene glycol (DEG) was integrated into the interfaces of the ZnO nanoparticles, as evidenced by X-ray photoelectron spectroscopy (XPS), and Fourier-transform infrared spectroscopy (FTIR), and ordinary solvents were unable to wash DEG molecules. The existence of DEG enhanced the dispersion stability of an aqueous suspension of ZnO nanoparticles in the absence of stabilizers [41].

Shahi et al. utilized the acidic p-toluene sulphonic acid-choline chloride DES as a template and hydrolyzing agent to produce titanium dioxide nanoparticles. They proved that the concentration of DES had a significant impact on the phase configuration of TiO_2. The pH of the solution was reduced by increasing the amount of acidic DES, which influenced the interactions between [TiO_6] components during the hydrolysis step. As the acidity of the mixture falls, the likelihood of the appearance of edge mutual bonds increases, potentially favoring TiO_2 anatase phase development, seen in reactions with 3 and 6 mL of DESs. In the synthesis procedure with the highest concentration of DES (12 mL), increasing the acidity of the medium causes the rutile phase composition to rise [40].

Because DESs are composed of hydrogen-bonds interactions, they are highly water-soluble and readily tend to capture moisture. Their desire to absorb water is inevitable and affects the physicochemical characteristics of DESs, such as the viscosity and melting point. Some studies took advantage of this property of DES and attempted to provide a water/DES system whereby viscosity of the mixture was reduced. Decreasing the viscosity is favorable for mass transfer through the synthesis processes to increase the yield. However, the volume of water used for such applications should be precisely considered because large amount of water can diminish the H-bonding in DES and may completely deform it [71,72].

According to Shahi et al. study, in their facile sol-gel method, tetra butyl titanate (1 mL) was added dropwise to different concentrations of the DES (3–12 mL), followed by adding H_2O (5 mL). They employed double distilled water through their technique, which may affect the DES nanostructure. In other words, the amount of water reported was 5 mL for all sets of experiments; however, for example, a rough estimation reveals that the W/W of water to the DES was approximately 1.6 times when 3 mL of DES was applied. Nowhere in the text, they discussed the effect of water in their study; however, it could have influences on reaction steps and, consequently, on physicochemical properties of prepared catalysts. Gutiérrez-Hernández et al., for example, surveyed the influence of DES ChCl: PTSA and the same one with H_2O in the Aza-Michael addition of arylamines to maleimide to acquire aminopyrrolidine-2,5-dione products. Through H/D exchange NMR investigations, they discovered that the mixture of water and DES maintains the transition states more than the DES-based reaction (around ten times) and leans the enthalpy-driven binding. It should be noted that such effects were observed when the W/W of water to the DES was only 0.5 [73].

Employing DESs (nonaqueous media) as electrolytes for anodic dissolution of metals through the electrochemical synthesis processes demonstrated sustainable method for attaining MOs [53,55]. Anicai et al. proposed a technique in which the anodic dissolution of Ti using a DES-based electrolyte and instant hydrolysis of DES to prepare nanosized TiO_2 was investigated (Scheme 2). They utilized ChCl: urea and ChCl: ethylene glycol (EG) electrolytes, in which faradaic efficiencies of 95–98% and 92–95% were determined, respectively, under the operating conditions, including applied current densities ranging from 2 to 7 A dm^{-2} and temperatures between 30 and 60 °C. After calcination at 400–600 °C, the catalyst exhibited an anatase phase with a narrow size distribution of 8–18 nm and bandgap energies in the range of 2.82–2.93 eV, which are lower than those of conventional TiO_2. The bandgap narrowing resulted from the excess oxygen in Ti nanostructure. Their discoveries indicated that the synthesized TiO_2 nanopowders might be able to be activated under visible light irradiation [42]. Similarly, Jia et al. reported the feasibility of preparing N and P co-doped narrow--band-gap TiO_2 (2.67–2.78 eV) by using choline phosphate: urea DES as the electrolyte. The HR-XPS demonstrated the doping or co-doping of N and P into the TiO_2 lattice. The existence of the non-metal impurities was attributed to DES itself, N/P including organic molecules, and/or groups derived from the disintegration of DES [53].

On the other hand, the utilization of DES for electrochemical applications can raise concerns, which have to be precisely assessed [18,74,75]. For instance, Haerens et al. reported that poisonous substances, such as dioxanes and chloroform, were produced by the electrochemical disintegration of ChCl and glycerol [76–78].

The etching and intercalation were the most recent functions of DES in AOP's catalysts, indicated by Song et al. considering Ti_3C_2 MXene-derived heterojunction photocatalyst [47] (Scheme 3). MXenes, a recent generation of 2D transition metal carbide or nitride (TMCs and TMNs, respectively), can function as outstanding catalyst support because of improving electron-hole separation and transfer and catalyst uniformity [79,80]. Typically, MXenes are yielded by etching out the "A" group element from MAX ceramics with the general formula $M_{n+1}AX_n$, where M symbolizes early transition metals, A stands for elements from IIIA or IVA groups of the periodic table, X represents C and/or N, and n equals to 1, 2, or 3 [81]. Song and co-workers prepared three DESs, ChCl: Hexafluorophosphoric acid (HPF6), ChCl: tetrafluoroboric acid (HBF4), and ChCl: trifluoromethanesulfonic acid (CF3SO3H) with molar ratios of 1:1, 1:2 and 1:3, respectively. Amongst the DESs, HPF6 indicated a desirable selective etching function.

Regarding photocatalytic activity, in-situ build-up of TiO_2 on Ti_3C_2 MXene can considerably boost e^-/h^+ pair separation and

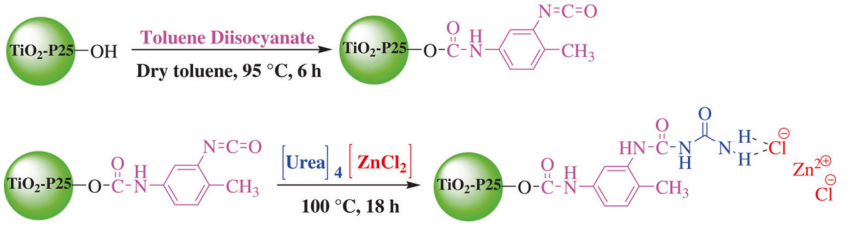

Scheme 1. Synthetic diagram of n-TiO2-P25@TDI@DES photocatalyst [59].

transfer thanks to the remarkable conductivity of Ti_3C_2 [82]. Besides, such an in-situ grown technique that leads to forming MOs from the support through exsolution proved higher attachment than those placed on the substrate surface via physical modification [83]. However, the c-lattice parameter of Ti_3C_2≈20 Å, meaning super narrow spaces of interlayers, restricts the in-situ formation or intercalation of typical nanosized catalysts (10–100 nm) [84]. Hence, Song et al. illustrated that DES can act as an intercalator to expand the interlayer of MXenes. The measured c-lattice parameter of Ti_3C_2 prepared in the DES was 38.02 Å, which means approximately two times larger than Ti_3C_2 utilized HF (20 Å). The intercalation influence of choline cations was responsible for the enlargement of the c amount [47,85].

Through DESs-assisted wet-chemical synthesis, Jaihindh et al. prepared hierarchical photocatalysts. In their study, DESs acted as a structure-directing agent and latent supramolecular catalysts. When DESs were added to the mixture of $Bi(NO_3)_3{\cdot}5H_2O$ and NH_4VO_3, the Bi^{3+} were readily linked with Cl^- and a pair of electron of oxygen atoms. Moreover, the existent VO_3 ions contributed to the bonded Bi^{3+} ions. The molecules of citric acid and choline as well as H_2O in the reaction mixture were able to develop strong Bi–O interactions while simultaneously H bonding with Cl^- qualifying them to enter the larger H bonding configuration. Notably, citric acid bound Bi by developing an H bonding lattice with H_2O [48]. Still, more advanced research is required to fully comprehend the DESs features in structural development.

By focusing on precursor role of DESs, Wu et al. fabricated a well-structured organic and inorganic complex with significant photocatalytic properties. Typically, they used a 0.5 mmol of Ga_2O_3, 1.0 mmol of 4,4′-bipyridine (bpy), 10.0 mmol of $H_2C_2O_4$, 5.0 mmol of choline chloride, and 5.0 mmol of HF at 140 °C for 72 h in a Teflon-lined stainless-steel autoclave (The Ga yield was 62.8%). They showed that the reaction of bpy and decomposed ionic component of ChCl: oxalic acid DES formed deprotonated bpy cations (H_2bpy^{2+}), shaped crystallized rod-like structure. By the single-crystal X-ray diffractometer (XRD), a 1D coordination rod-like framework, templated by H_2bpy^{2+}, was observed. In fact, two $C_2O_4^{2-}$ and a GaF_2O_4 octahedron assembled the unlimited anionic $[GaF(C_2O_4)_2]^{2-}$ rod-like structure, and positive charges of H_2bpy^{2+} neutralized the anionic portion (Scheme 4). Moreover, The Ga–O and Ga–F gaps (1.9287(16), 1.90635(10) Å, respectively) point to the specific location of Ga [60].

5. Physical properties of catalysts affected by DES

A different kinds of methods have been used to synthesize nanosized catalysts, such as chemical precipitation, sol-gel method, hydrothermal synthesis, and physical or chemical vapor deposition [40,42]. Since the size and morphology of nanostructures are affected by preparation and synthesis conditions with important role of solvents. Several studies focused on developing of procedures allowing to control the structure and morphology of synthesized catalysts to improve their capability and efficiency [38,41,86,87].

As previously mentioned, several functions can be assigned for DESs in synthesis processes, such as stabilizing agent [41], capping agent [36], solvent [44], hydrolyzing agent [40], structure director [36], and growth controller [40]. Some studies also suggest multifunctional DESs acting simultaneously as a solvent, reactant, and template in the synthesis of AOP catalysts [39].

The benefits of DESs improve and enhance the physical properties of the resulting catalysts. Consequently, their efficiency in the removal of intended pollutants from water matrix is perused by different studies [41,43,45]. The enhancement in physical properties of

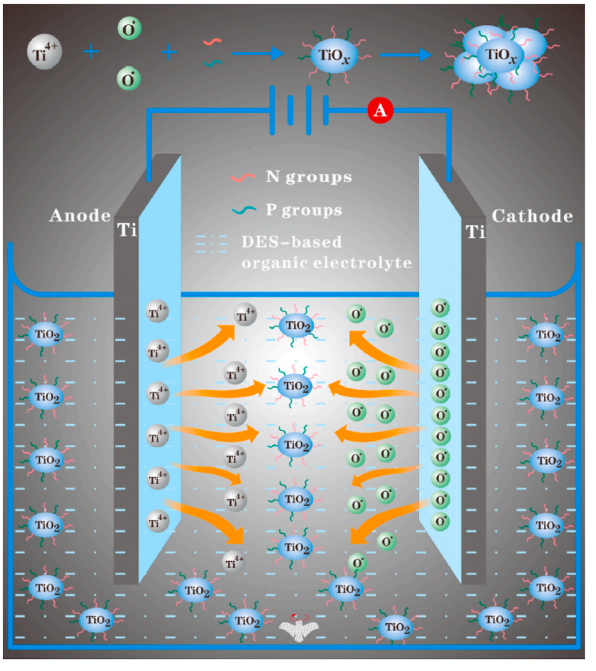

Scheme 2. Mechanism process of DES-based electrolysis technique for the synthesis of N/P-loaded TiO_2 [53].

synthesized catalysts should be assessed by advanced techniques to capture a clear vision of catalyst behavior. For example, since some catalytic degradation processes should adsorb the pollutants on their catalytic surface, the specific surface area (SSA) could be a fundamental parameter to measure the adsorptive behavior of the catalyst [35]. For instance, synthesized TiO_2 NPs by ChCl/p-toluene sulphonic DES revealed to possess higher photocatalytic efficiency in methyl orange removal with a higher surface area than that of commercial photocatalyst Degussa P-25 [40].

In this regard, the morphological properties of synthesized catalysts have been assessed by Scanning Electron Microscope (SEM), Transmission Electron Microscope (TEM) [35], Field-Emission Scanning Electron Microscope (FESEM) [43], Brunauer-Emmett-Teller (BET) [42], and Barrett-Joyner- Halenda (BJH) techniques [37].

SEM techniques are practical methods to investigate surface texture of particles. TEM analyses are also used to determine the size distribution, surface morphology, and structural imperfections [35]. High specific surface area and pore volume are fundamental parameters in the efficiency of nanocatalysts, which are assessed by means of BET and BJH analysis, respectively [37,40]. In the following, we investigated the articles to find the effects of DESs on the morphology and surface area of the catalysts synthesized with and without DESs.

DESs as green materials can be a trustworthy alternative for common organic and inorganic hazardous solvents and other toxic chemicals used in catalysts synthesis [38,40,56]. One of the advantages of DESs is that they can dissolve most metallic compounds [43, 44,47]. The metal oxides-based catalysts are widely employed in AOPs due to their outstanding properties and high effectiveness [37, 59]. Therefore, many researchers assess the use of different kinds of DESs as solvents in the synthesis of MO-based catalysts with desired structure [43,44].

As discussed earlier, applying water while using DES as the solvent can adjust DES's properties, such as viscosity and H-bonding network, and consequently change the DES effect through the synthesis process. With this regard, Devi and Singh used ChCl: EG DES to fabricate Mn_2O_3 flower-shaped nanoparticles with facet structures that showed high catalytic efficacy. In their study, DES acted as a capping agent, and various morphologies of NPs with different water content in DES were obtained. Studied ratios of water to DES for samples 1, 2, and 3 were 0/2, 0.5/1.5, and 1/1 V/V, respectively. SEM results indicated that the decrease in DES concentration significantly changed the morphology of the samples. For instance, DES that contained no water allowed to obtain bonded spherical configurations. However, by adding water (sample 2), a flower-shaped catalyst was formed. Interestingly, when the water to DES ratio was 1/1 V/V, spherical shapes were reconfigured, but no bonding was detected [86]. Probably it follows from the fact, that above 40% content of water, the DES does no longer exist. In such conditions, the DESs loses its properties and a solution of HBA and HBD in water exists.

The DESs/water/MOs system can constitute an antisolvent process in which MO nanostructures with tunable properties can be generated. Dong et al. employed a DES-based antisolvent technique to develop both single-crystalline and mesocrystal structures of ZnO by means of ChCl/urea DES as the solvent [43,44]. In the synthesis of ZnO a mesocrystals, i.e. formation of the nanostructures was facilitated by adding tris(hydroxymethyl)aminomethane (Tris) in different amounts to water, resulting in mesocrystal by controlling the crystal growth in specific directions [44]. Single-crystalline, ultrathin, and mesoporous ZnO nanosheets were also produced through this method followed by calcination. In this proposed method, ZnO-containing DES served not only as a solvent but also as the ZnO precursor, producing non-porous crystallographic structures that calcination of which resulted in single-crystalline, mesoporous ZnO nanosheets. It is also noteworthy that prepared by this method products showed higher specific surface areas and smaller nanosheet thicknesses than that of microwave-assisted and hydrothermal processes [43]. Both ZnO products exhibited high photo-catalytic activities comparable with commercial P-25 TiO_2 [43,44].

Magnetite (Fe_3O_4) nanoparticles (MNPs) are other kinds of catalysts that are widely applied in AOPs [45,46]. ChCl/urea DES was also studied as a solvent for the synthesis of Fe_3O_4 MNPs. In comparison with other common solvents such as water and ethylene glycol, DES-assisted synthesized Fe_3O_4 MNPs revealed to have a spherical structure with larger BET surface areas, resulting in superior catalytic performance. In fact, DES act as a reaction medium to control the nucleation and growth of MNPs and stabilizes the particles via adsorption of choline cations [46]. Likewise, Sri et al. utilized choline chloride and citric acid-based DES to synthesize cubic shape

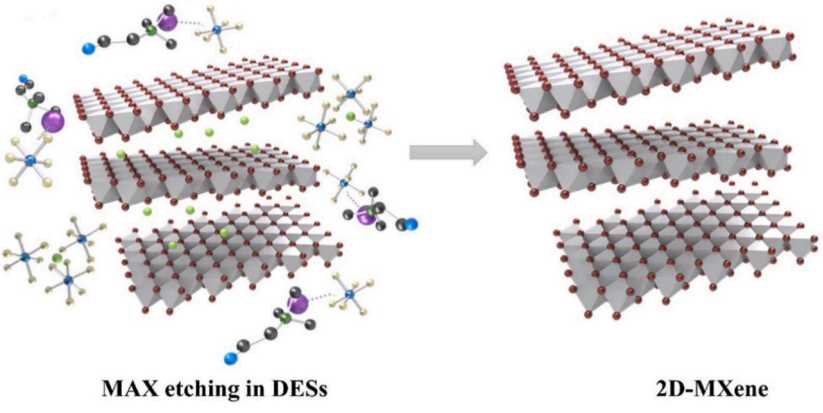

Scheme 3. Synthesis mechanism of MXenes by DESs method [47].

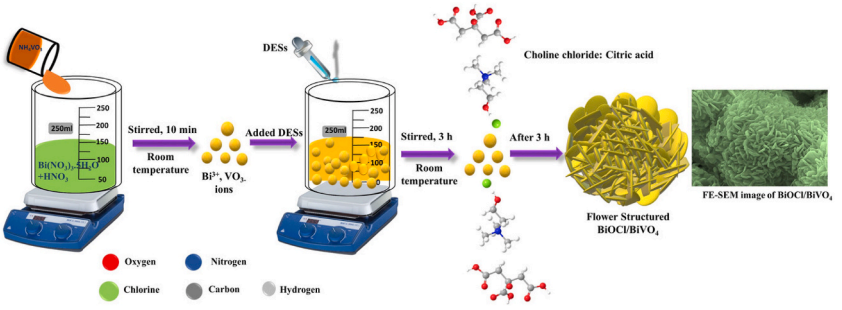

Scheme 4. a) building units of compound 1-A; b) infinite anionic $[GaF(C_2O_4)_2]$ chain built from GaF_2O_4 octahedra and two oxalates; c) *N*–H···O H-bonding interactions of $|C_{10}H_{10}N_2|[GaF(C_2O_4)_2]$ along the [001] direction. Color: O, red; C, gray; H, white; N, blue; F, powder-blue; Ga, green [53].

MNPs. Employing ChCl/citric acid DES hindered the agglomeration of particles, resulting in the development of crystallite cubic nanoparticles with the mesoporous structure, confirmed by SEM and high resolution TEM analysis [45].

Karimi et al. applied ferric chloride-choline chloride DES that simultaneously acted as a solvent, reactant, and template in the synthesis of hematite nanoparticles [34]. Based on their study, the high ionic strength of DES caused the controller growth role and prevented the agglomeration of particles. The calcination of fabricated products increased the crystallinity, although as-synthesized nanoparticles exhibited more activity in the degradation of RhB compared with calcined ones [39]. Such a "growth control" role was also observed in the synthesis of TiO_2 nanoparticles, where the DES acted as a capping agent to form the active facets in special directions [36] or favorable coral-like structures [40]. The growth inhibitor role of CTAB and acetic acid DES in the synthesis of ceria NPs resulted in a highly mesoporous structure with more porosity and surface area in comparison to conventional synthesis methods [37]. Relevant results were also observed in the fabrication of amorphous Fe NPs by means of ChCl and sucrose-based DES, which caused a mesoporous structure with a high surface area of 20.9 $m^2\ g^{-1}$ [35].

In spite of the wide usage of TiO_2 and ZnO, numerous efforts have been conducted to improve the catalytic efficiency by employing DES-based electrolysis method along with doping metal or non-metal additives [53,55–57].

Anicai et al. synthesized TiO_2 nanopowders by DES-based electrolyte and the results indicated that prepared TiO_2 nanopowders had surface area values higher than that of commercial products with mesoporous structure [42]. In 2019, Danilov et al. studied the fabrication of Ni–TiO_2 composite by means of electrolytes comprising ChCl/EG DES [55]. According to their study, suspension of TiO_2 nanoparticles in the DES-based electrolyte affects the growth and formation of metal crystallites. Therefore, application of DES-based electrolytes guarantees the uniform distribution of nanoparticles within a metal matrix while reducing the agglomeration of nanoparticles [55]. Accordingly, preparation of non-metal (N and/or P) co-doped TiO_2 by using the DES-based pure organic solution as the electrolyte was proposed by Jia Haiyang et al., in 2021. The DES used in their study was a mixture of choline phosphate and urea with the role of charge transfer. In fact, in their proposed method named as DES-electrolysis strategy. The DES or its decomposition products adhered to TiO_2, and with the calcination of consequent substances, N and/or P co-doped crystalline TiO_2 was formed. Based on morphological characterizations, all the samples showed irregular ellipsoids or capsule-like shapes with rough surfaces and monocrystal characteristics. The highest specific surface area was obtained at the calcination temperature of 500 °C (26.1 $m^2\ g^{-1}$), while by increasing the temperature, SSA decreased and reached 5.3 $m^2\ g^{-1}$ at 800 °C.

Utilizing support materials such as graphene oxide (GO) or neat graphene (NG) can provide numerous benefits namely, enhancing surface area and recycling, which improve the catalysts efficiency using dedicated support materials. It is widely evidenced that the photocatalytic efficiency of ZnO/graphene is improved in comparison with pure ZnO. Due to the hexagonal sp^2 carbon lattice of NG, it is more chemically stable and electrically conductive compared to GO. However, polar functional groups on the surface of NG, which severely impact NG's capability to be processed in water, are inadequate. As a result, many existing wet chemical routes for the preparation of ZnO/graphene are unsuitable. To obtain uniformly sized and distributed nanocatalysts via the aqueous chemical route, additional agents such as surfactants are essential, which results in extra costs and risks to the environment. Therefore, the simple green method employing DESs for producing ZnO/NG non-hybrids was proposed [56,57]. Accordingly, Jin et al. employed choline chloride/diethylene glycol (ChCl: DEG) as a reaction medium to synthesize ZnO/NG. Based on TEM analysis, the presence of graphene significantly affects the size and uniformity of ZnO that were evenly distributed on the graphene sheets. On the other hand, BET analysis revealed that due to the incorporation of NG, surface area and total pore volume of ZnO/NG improved 5 and 10 times than those of the pristine ZnO nanoparticles, respectively. All these benefits were achieved in the light of using the DES. In other words, for controlling the morphology of ZnO, no water and additional chemicals were employed in the synthesis of ZnO/NG. Moreover, DES provided a desirable condition in which the in-situ assembly of ZnO particles onto graphene nanosheets was accomplished in a single setup [57].

MXenes are the next generation of two-dimensional transition metal nitrides or carbides that support the uniform growth of catalysts. Increases in the interlayer spacing and c-lattice parameter of MXenes might enhance the photocatalytic performance of MXenes-derived photocatalysts. HF or HCl/LiF, both of which are highly hazardous, are commonly used to obtain this structure. Therefore, the synthesis of intercalated MXenes could be replaced by DESs with component-designability and solvent characteristics toward metallic elements. Song et al. investigated the effect of three distinct DESs, namely ChCl-HBF_4, ChCl-CF_3SO_3H, and ChCl-HPF_6, on the synthesis

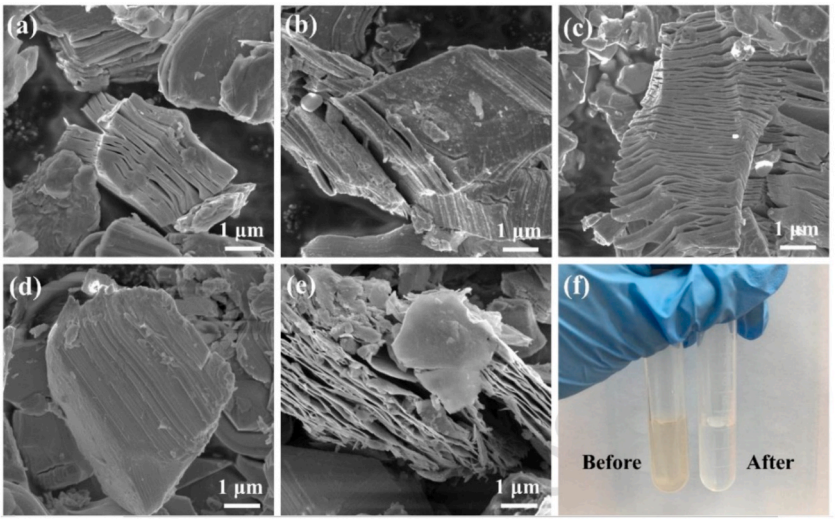

Fig. 2. SEM Images of synthesized Ti_3C_2 in several DESs with different molar ratios (a) ChCl: HBF_4 (1:2), $ChCl:CF_3SO_3H$ (1:2), $ChCl:HPF_6$ (1:2), ChCl:HPF6 (1:1), ChCl: HPF_6 (1:3). (f) The DES photos prior to and following reaction (47).

of Ti_3C_2 MXene. ChCl-HPF_6 with a molar ratio of 1:2 produced the best-defined accordion-like structure with the most interlamination, based on SEM images (Fig. 2). In fact, DES as a solvent, significantly increased the morphological and structural properties of Ti_3C_2 MXenes. In addition, unlike the conventional HF or HCl/LiF technique, DES serves as the buffering layer, alters the surface, and mediates the severe etching response. In the end, the synthesis of Ti_3C_2 MXenes with enlarged interlayers promotes the formation of TiO_2 crystals on Ti_3C_2 structures, hence enhancing the photocatalytic performance of MXenes-derived photocatalysts [47].

One of the other catalysts that are widely used in the photodegradation of pollutants is bismuth vanadate ($BiVO_4$) because of its outstanding features such as narrow band gap (bandgap: 2.4 eV) [48,50,52]. The photocatalytic activity of $BiVO_4$ catalysts is highly affected by the structural properties of particles, which depend on the chemicals used in the synthesis process [52]. Many studies have been done to replace the toxic and acid-alkali chemicals in the synthesis of $BiVO_4$ catalysts by DESs [48,50–52]. The production of $BiVO_4$ spindly microtubes by choline chloride: urea DES was studied for the first time in 2010. Based on SEM analysis (Fig. 3), microtube structures consisting of uniform particles were observed with the rough internal surface for hallows that were rarely reported in other studies for similar tube-shaped materials. These defects increase the effective surface area and consequently enhance the photocatalytic performance of the catalyst. The DES acted as structure-directing agent, but also as it adsorbed on the surface of microtubes, it controlled the growth and nucleation of particles resulting in single-crystal $BiVO_4$ spindly tubes with a high surface area [51,52].

To improve the catalytic performance of $BiVO_4$, a number of studies have attempted to enhance its morphological structure and construction by synthesizing ternary heterojunctions and hierarchical structures using DES-assisted techniques [48–50]. Accordingly, Jaihindh et al. used choline chloride/urea DES as a reaction medium to synthesize hierarchically nanostructured $BiVO_4$. Although, based on literature, the morphology of $BiVO_4$ is tunable by controlling the pH, temperature, and surfactants, the well-crystallized shuriken like $BiVO_4$ with hierarchical structure and a high surface was synthesized by means of DES with the role of morphology controller [49]. DES-based methods were also used to fabricate ternary heterojunction $BiOCl/BiVO_4$ [48,50]. In the presence of water, DES components can act as latent supramolecular by bringing reactive elements together with more tight bounds. For example, ChCl: citric acid DES with the role of latent supramolecular was utilized as structure-directing, facilitating the formation of the

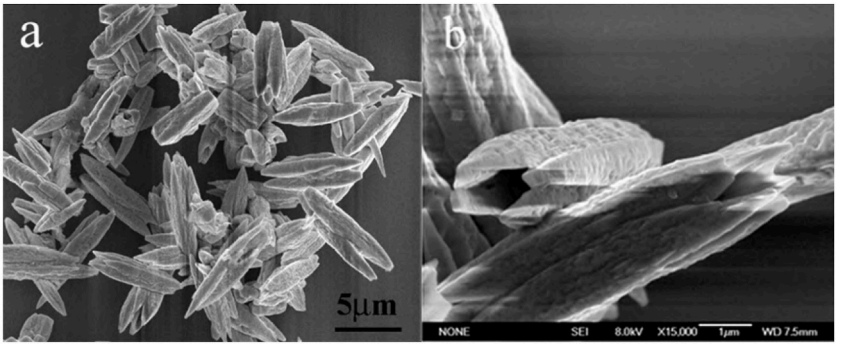

Fig. 3. *(a) SEM image of the as-obtained product at low magnification; (b) Close view of microtubes revealing their hollow structure and wall thickness (52).*

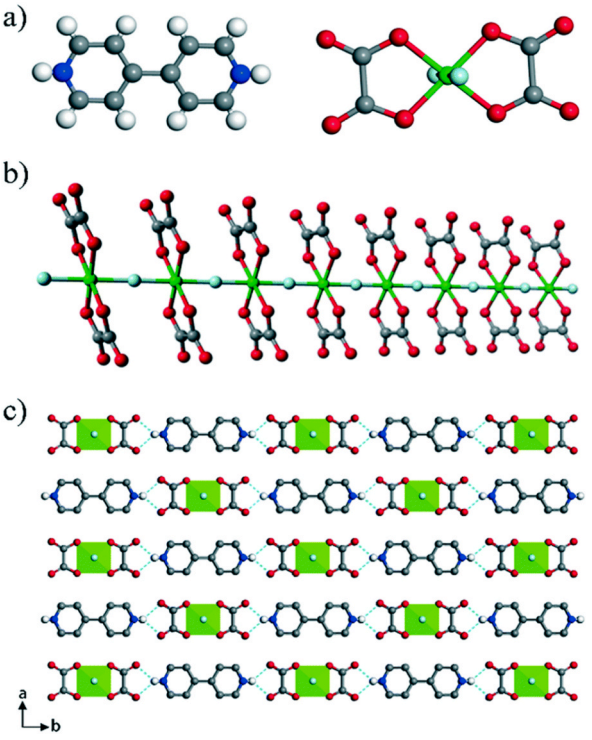

Scheme 5. DES assisted wet-chemically synthesized $BiOCl/BiVO_4$ [48].

flower-structured $BiOCl/BiVO_4$ (Scheme 5). Citric acid and choline molecules, along with water molecules make a favorable solution to form Bi–O bonds and simultaneously hydrogen bonding with chlorides. Accordingly, reactive elements are bound together tightly which facilitates the flower structure growth [48]. In the synthesis of ternary $BiOCl/BiVO_4$, nanosheet-structured microparticles with smaller sizes were observed when particles were synthesized with the DES in comparison with the non-based DES approach [50]. The possibility of using DESs as green solvents for the synthesis of other ternary metal oxides was also studied where mesoporous structures with sound morphological properties were obtained [32].

Other types of photocatalysts are utilized in semiconductor-based photocatalysis, including metal sulfides (MS) and metal chlorides (MCl). In the synthesis of such catalysts, DESs, which are environmentally friendly solvents, can serve as a source of sulfur and chlorine. On the other hand, when the synthesis of MCl and MS catalysts utilizing DESs was explored, it was discovered that DESs play a multifunctional role [33,58]. When Ge et al. used ChCl: urea to fabricate Ag@AgCl, results revealed that the DES not only acts as a solvent and Cl source but also as a reducing agent for the formation of Ag^0 nanoparticles. The AgCl that is created when NaCl is utilized as the source of Cl has a spherical form, and relatively few metallic Ag^0 nanoparticles are produced during this procedure. These findings provide more evidence that DES acts as a reducing agent in the process of producing Ag^0 nanocatalysts [58]. Likewise, same multifunctional performance was observed for DESs in the DES-assisted synthesis of $CdS@CeO_2$ composites. Owing to hydroxyl groups, polyethylene glycol (PEG) acts as a growth controller to develop certain crystal faces (Fig. 4) [33].

Deep eutectic solvents have been also used to synthesize carbon-based materials such as biochar and inorganic-organic complexes; however, they were less investigated compared to other types of DES-assisted catalysts [34,60]. For example, Wu et al. employed a DES system to synthesize in inorganic-organic complex $|C_{10}H_{10}N_2|[GaF(C_2O_4)_2]$ with photochromic behavior and tunable photocatalytic activity [60]. The structural and surface properties of biochar-based catalysts, as well as other forms of organic-based catalysts used in AOPs, can be improved by using deep eutectic solvents.

According to the research carried out by Ye et al. ChCl: urea DES was utilized in fabricating *N*-doped refined biochar (NRBF) in order to circumvent any potential barriers. The filamentous structure of virgin biochar is destroyed during the DES processing method, and surface modification of derived biochar is achieved with the addition of nitrogen. As a direct consequence of this, NRBF was effectively synthesized with a fibril structure and a larger surface area when compared to pristine biochar [34]. DES-modified biochar was examined by SEM, as indicated in Fig. 5. Both, pristine biochar and NRBF, catalysts inherit the rod-like structure of Ramie fiber. Fig. 5a and b demonstrate that interconnected filaments accumulated and condensed to produce one-way directed channels on the pristine biochar. Following DESs treatment, the connected and surface anchoring substances of filaments were destroyed, leading the 200-nm diameter refined fibrils to be isolated. DESs were responsible for the effective separation of fibrils from fiber biomass due to their swelling processes and intercalation effect. Since DESs can infiltrate fiber filaments and reduce the binding energy between fibrils by decreasing the hydrogen H_2 bonds, diminishing their hydrophobic affinity, and eliminating related substances [88,89]. Hence, the

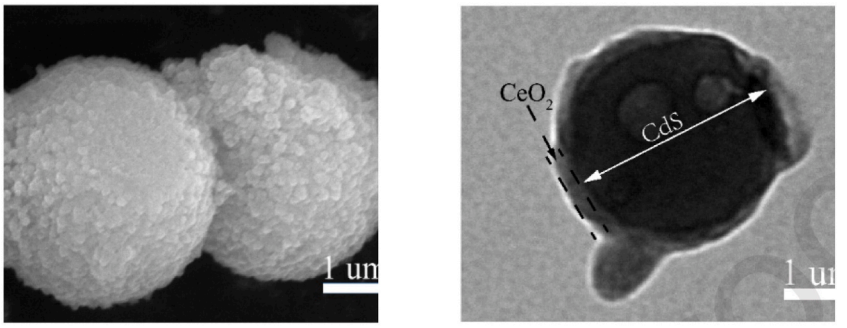

Fig. 4. *SEM (a) and TEM (b) images of CdS@CeO_2-1 (the depicted catalyst was prepared in PEG 200: thiourea DES through the solvothermal technique in which the molar ratio of CeO_2 to CdS was 1:1 (33).*

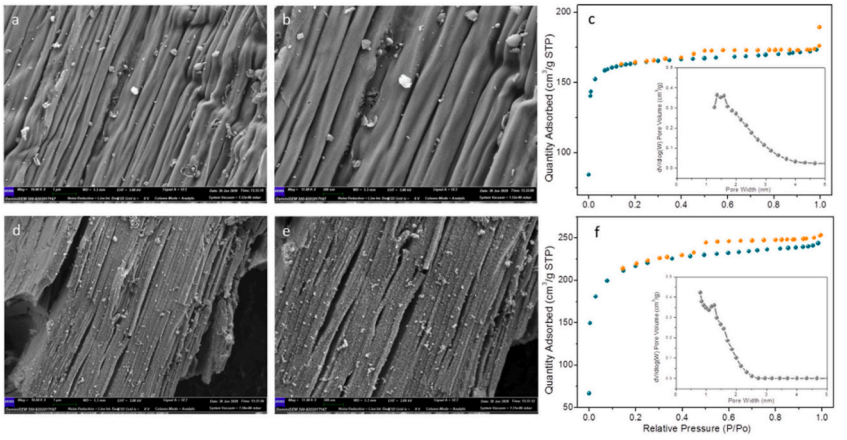

Fig. 5. -SEM images of pristine biochar (a and b) and the N2 adsorption-desorption isotherm (c), along with the inserted curve of pore size distribution. SEM images of NRBF (d and e) and the N2 adsorption-desorption isotherm (f), along with the inserted curve of pore size distribution (34).

refined fibrils would be isolated from the entire biomass fibers [34].

Moreover, Fig. 5c and f illustrate the N_2 adsorption-desorption isotherm and pore size distribution of biochar-based catalysts before and after modification. Both biochar exhibited I/II-type isothermal curves with a sharp adsorption inflection at low pressures. Tiny fissure holes in filamentous structures were found to have hysteretic loops of type H4 in the desorption branch isotherm. NRBF indicated a larger BET-specific surface area than pristine biochar, 565 and 479 $m^2\ g^{-1}$, respectively. Further, the micropore area of NRBF was calculated by the t-plot technique, which was 3.12 nm, while the virgin one indicated a 2.05 nm micropore area [34,90]. It was proved that DESs could enter comfortably into the filamentous configuration, thus also expanding the distance between each fibril or accomplishing the disconnection of the filament arrangement through swelling and partial dissolution of the interconnected compounds, thereby producing plenty of micropores in the fissure [34].

Due to the outstanding tunable morphological and structural features of the biochar-based catalysts, they can be a perfect candidate to be investigated through further research by introducing other types of DESs to direct and improve their morphological properties and surface area.

6. Chemical properties of catalysts affected by DES

The chemical properties of DES-assisted catalysts are usually assessed by several characterizing methods such as XRD, XPS, and FTIR. Herein, we attempted to consider the effect of DESs on the chemical properties of catalysts by focusing on structural analyses.

According to available literature, DESs can act as ideal structural directing agents for handling the synthesis of nanocatalysts with high-index surface planes [36,48]. Due to high active catalytic sites, high-index planes have the potential to accelerate both direct and indirect catalytic degradation routes. As a result, high-index planes have greater activity than basal planes; nonetheless, because of the rapid generation of destructive by-products, inferior activity can take place at low potential [91].

Sun et al. fabricated an electrode by forming antimony-doped tin oxide (Sb–SnO_2) coating on Ti substrate in two different electrolytes, DES and deionized water (Ti/SnO_2–Sb-DES and Ti/SnO_2–Sb-DW, respectively). X-ray diffraction pattern was used to evaluate the crystal structure of coated Ti/SnO_2–Sb-DES and DW, indicating the tetragonal phase of SnO_2. Due to the broader half-peak width of

the electrode prepared in DES comparing to the other one, smaller crystallites were proved, indicating more active sites to improve electrocatalytic activity. Since the DES-based electrode exhibited a diffraction signal weaker than Ti/SnO_2–Sb-DW, it can be assigned to the homogeneity of the coating covering, which boosts Ti/SnO–Sb-DES electrode electrochemical activity and durability [61].

Among the gathered studies, only Shahi et al. investigated the concentration of DES on the phase of resulting catalysts. In doing so, acidic DESs (ChCl: p-toluene sulphonic acid (PTSA) with 1:1 M ratio) in various concentrations, i.e., 3, 6, 9, and 12 mL, were applied to fabricate TiO_2 nanocatalysts [40]. They proved that increasing the concentration of acidic DES resulted in a reduction in anatase. For example, the prepared samples with DES concentrations of 3 and 6 mL indicated a 100% anatase phase; however, only 34.7% of the same phase was formed in DES concentration of 12 mL. On the other hand, the formation of the rutile phase was observed with 28.4% in sample DES-9-mL and 65.3% in DES-12-mL. Above 600 °C, the samples that contained the highest concentration of DES indicated a complete transformation from anatase to rutile phase. However, for the rest of the samples, complete conversion into the rutile phase did not occur, resulting in anatase–rutile mixtures with an increase in rutile content.

XRD analysis demonstrated that DES concentration adjusted the phase structure of TiO_2 nanoparticles. By raising the concentration of acidic DES, the acidity of the solution grew, hence altering the composition of the TiO_2 phase. It was previously discussed that in solutions, Ti(IV) complexes appear as octahedrally coordinated complex ions, and the acidity influences the bonding between [TiO_6] structures constructed during the hydrolysis of the TiO_2 precursor. Reduced acidity of the solution improves the likelihood of edge-shared bonding, which might promote the development of the TiO_2 anatase phase. On the opposite side, the higher acidity of DES-12-mL enhances the rutile phase composition.

Moreover, UV–Vis diffuse reflectance spectroscopy (DRS) was conducted, and, however, a slight reduction was detected in DES-assisted synthesized TiO_2 (3.0 eV) compared to commercial TiO_2 Degussa P-25 (3.1 eV) [40]. By contrast, other investigations showed a significant shift into the visible region. Taghavi et al. for example, functionalized nano-TiO_2-P-25 b y a linker, 2,4-toluene diisocyanate (TDI), and DES (urea: $ZnCl_2$). The DRS indicated that the band gap energy of the modified TiO_2 was placed in the visible region (2.55 eV). By comparing to nano-TiO_2-P-25-modified TDI, the DES significantly affected the band gap energy due to the Zn^{+2} ions added to the catalysts [59]. The results indicated that the why and how DESs used in the synthesis procedures can considerably influence the final products. Hence, attention to the roles of each component of DESs can assist future studies in achieving their objective.

Another interesting study in which DES served not only as an electrolyte but also as a doping agent was conducted by Jia et al. [53] The effect of different temperatures was investigated on the N and P co-doped TiO_2. The authors utilized phosphorus-based DES and calcined the samples at various temperatures of 500, 600, 700, and 800 °C, named T-5, T-6, T-7, and T-8, respectively (Scheme 6). HR-XPS suggested that N and P were electrolyte-derived elements. Three states were derived from T-5 and T-6 N1s spectra (Fig. 6a and b). Ti–O–N in TiO_2 was ascribed with singles at 399.7 and 399.6 eV for T-5 and T-6, respectively. Further, peaks of 401.6 and 400.6 eV for the calcined sample at 500 °C and 400.3 and 401.0 eV for prepared ones at 600 °C were related to C–N/C NHx and N–O in NOx, respectively. Extreme calcinations simplified nitrogen's chemical states. T-7 sample did not contain N–O bonds in NOx surface-chemisorbed species (Fig. 6c), while T-8 had only Ti–O–N bonds (Fig. 6d). The atomic ratio of N to Ti also dropped from 0.041 to 0.025 when calcination was accelerated, which was due to the fact that higher-temperature calcination released more N atoms, causing the drop. Moreover, due to less phosphorus than nitrogen in the electrolyte, P had less weight in the final product. Because of insufficient range and sensitivity discrimination, P 2p HR-XPS spectra was unable to retrieve a solid evidence for chemical bond details.

Literature reports that the thermal stability of DES-assisted catalysts can be improved because DESs are able to enhance the electrochemical stability of nanocatalysts. For instance, Iqbal et al. utilized two types of solvents, CTAB: acetic acid DES and acetic acid, to find those which displayed a better thermal resistance for resulting Ceria nanoparticles. Thermogravimetric (TGA) and derivative thermogravimetry (DTG) analyses of Ceria and DES-Ceria nanoparticles revealed that water vapors adsorbed on Ceria and DES-Ceria NPs were released. This weight loss was detected below 100 °C. Organic residual components lost 3–5% of their weight between 100 and 225 °C, the DTG curves centered at 78 °C and 207 °C for Ceria and 64 °C and 218 °C for DES-Ceria. For both prepared nanocatalysts, increasing the temperature from 225 °C to 500 °C boosted weight loss by about 15%. DES-Ceria nanocatalysts (T_{max}: 350 °C) were more stable than Ceria (T_{max}: 260 °C). This enhancement in Ceria nanocatalysts' thermal stability in DES could boost electrochemical stability [37].

7. Effect of process parameters on catalyst performance

As mentioned earlier, one of the key targets of this study is to define the application of DES-assisted synthesized catalysts for AOPs. Analysis of data compared in Table 2, reveals that the majority of the AOPs based on these materials are photocatalytic processes using MOs as the driving catalysts. Moreover, the focus of the studies was mostly on organic pollutants, especially dyes and pharmaceuticals. Herein, the five most operational parameters in AOPs have been compared. With respect to the catalyst dose and operating time, it is worth pointing out that most studies have reported the 0.5 g L^{-1} of catalyst dose and 120 min of treatment time as their optimal operational conditions, respectively. Although not only these two parameters but also other ones are affected and controlled by various factors, we attempted to provide a clear vision of the role of DES in operational parameters for AOPs.

According to studies that applied DESs for synthesizing catalysts, some differences were found between DES-assisted catalysts and those obtained in traditional/commercial way, which mainly attributed to DES effects on the physical and chemical properties of catalysts. Concerning the physical features, DES can change the morphological structure of the catalyst, which sometimes provides a higher surface area. Iqbal et al. synthesized the ceria nanoparticles in CTAB: acetic acid-based DES and acetic acid for the degradation of flumequine under UV irradiation [102]. They found a higher degradation rate for the DES-assisted catalyst (94%) than that for acetic acid (73%). The highly mesoporous and crystalline structure of DES-assisted catalyst was the most probable reason. The physical

change affects the operational parameters such as catalyst dose, light exposure, and pollutant concentration encouraging scientists to investigate them.

As mentioned in most of the reviewed literature [117–119], a higher dose of catalyst poses a higher photodegradation rate – up to some optimum. Overload of treated solution with catalyst particles causes high increase of turbidity which inhibits the light absorption by the solution as well as catalysts particles resulting in lower degradation effectiveness [27]. Due to the physical nature of the phenomena, it is also possible to follow this trend by the DES-assisted catalysts.

Xu et al. compared CdS synthesized by water and PEGylated DES as a solvent for degradation of tetracycline. They also prepared CdS@CeO_2 core-shell material through the solvothermal and calcination process at the molar ratios of 0.25, 0.5, 1, and 2 (CeO_2: CdS). Two synthesized CdS and four CdS@CeO_2 had the k values (degradation constant) of 0.01104, 0.02126, 0.02561, 0.02219, 0.03338, and 0.02672 min^{-1}, respectively. By comparing the corresponding k values for CdS (H_2O) and CdS, it can be proved that PEGylated DES is able to improve the photocatalytic activity [97]. Within this regard, Anicai et al. compared the degradation rate performance of DES-assisted TiO_2 nanopowders with the commercial one. Their results were in alignment with the previous study [109].

However, it can possible that the synthesize of DES-assisted catalysts leads to lower degradation rate. For example, Dong et al. [110] found an inhibitory role in relation to zinc carbonate hydroxide produced from the reaction of urea and Zn^{2+} during the antisolvent process. Indeed, calcined zinc carbonate hydroxide as layered hydroxide salts create voids which thermodynamically decreases the total surface area of the synthesized catalyst.

Therefore, it can be concluded that applying DES-assisted catalysts also leads to a short process time which reported as degradation time. For example, comparing commercial TiO_2 and TiO_2/ILEG-EtOH, it was found that complete degradation (Orange II dye) was in about 300 min for DES assisted catalyst, while the reaction time was more than two times higher for commercial one [109]. This effect is described more precisely in a study conducted by Cun et al. [41]. They reported almost complete degradation of MB in less than 60 min for ZnO nanoparticles synthesized in DES environment. In case non modified ZnO the degradation time was increased to 75 min. Studies on degradation mechanism, revealed that present oxygen vacancies promoted electron transfer and photocatalytic reactions. The same result was also obtained by other study [115], when the degradation efficiency of Fe_3O_4 catalysts synthesized by ChCl:2urea DES was compared by other methods (H_2O and MEG solvents) under a typical procedure of H_2O_2 adding as an oxidant. This procedure reveals another aspect of DES role in association with the oxidant applying on the process which has not been adequately investigated.

When the performance of Fe_3O_4 catalysts synthesized by DES was investigated, $^{\bullet}OH$ as the main reactive oxygen species were generated from H_2O_2 (a Fenton-like process). It was proved that DES-assisted synthesis resulted in a catalyst that was able to produce higher amounts of hydroxyl radicals. This assumption can be demonstrated by comparing the data related reaction rate coefficient, surface area, and site density obtained by Chen et al. [115].

The role of electromagnetic radiation as one of the main components of photocatalytic degradation is considered by many scientists. Since it is demonstrated that the catalyst synthesized by DES provides a higher surface area, various ideas in association with the role of light were applied during the time. The effect of the light source on the degradation rate of DES-assisted catalysts has been surveyed in different ways. However, this effect was usually tested after the period of dark adsorption, which was reported by many studies [97,98,100,103]. This approach usually is done to obtain an equilibrium of adsorption-desorption and estimate the amount of pollutant adsorbed on the surface of the catalyst. Ciğeroğlu et al. investigated the degradation of cefixime trihydrate under the dark condition, UV, and UV with DES-assisted ZnO/GO nanocomposite. The observed pollutants reaction rate constants have been determined to be 0.0086 min^{-1}, 0.0056 min^{-1}, and 0.0249 min^{-1}, respectively which indicated the considerable improvement of catalyst performance in case of DESs application during its synthesis. It was explained by its higher photocatalytic activity and higher surface area [95]. Based on reviewed studies, only Iqbal et al. exclusively investigated the effect of UV fluence over time (from 0 to 720 mJ cm^{-2}) at a constant fluence rate of 0.1 mW cm^{-2} on DES-assisted photocatalyst performance. The degradation rate of an antimicrobial agent under different conditions (sole DES-Ceria, sole Ceria, sole UV-C, UV-C/DES-Ceria, and UVC/Ceria) showed a direct relationship between UV fluence and degradation efficiency. The results indicated that using DES enhanced the UV light absorbance by

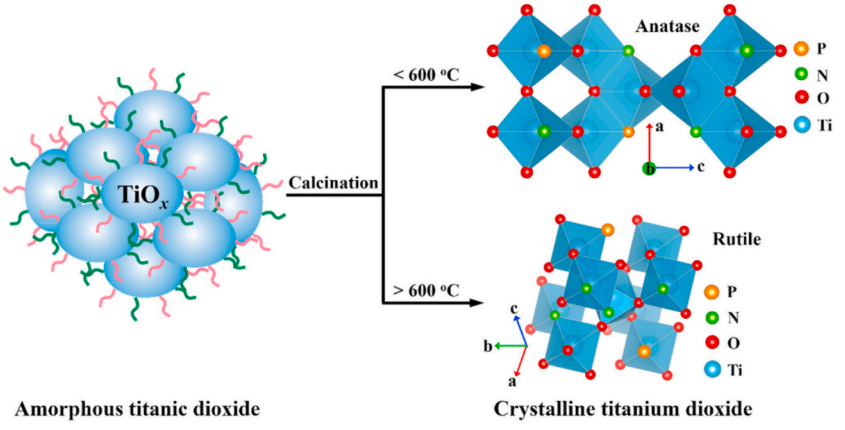

Scheme 6. The effect of calcination temperature on the structure of non-metal-loaded amorphous TiO_2 [53].

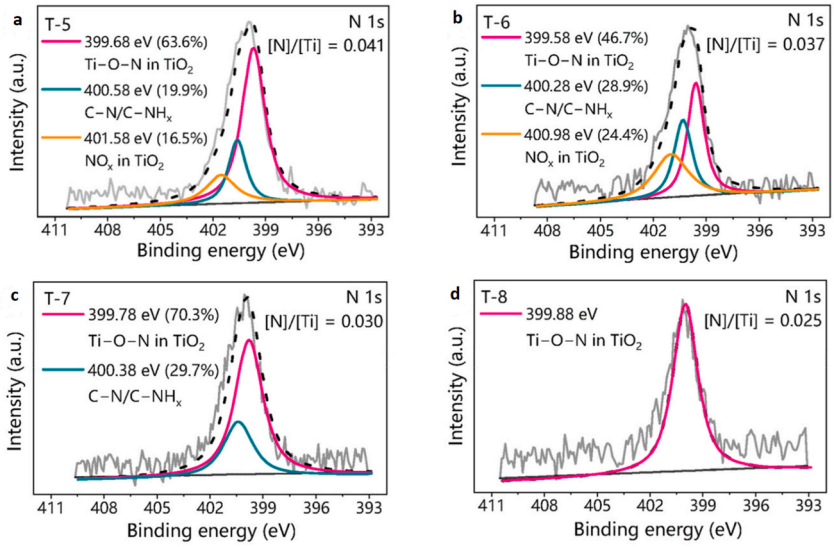

Fig. 6. HR-XPS spectra of N 1s in samples T-5, 6, 7, and 8 (calcination temperature: 500 °C, 600 °C, 700 °C and 800 °C respectively) [53].

catalyst UV/DES-Ceria, leading to 94% removal efficiency [102]. Missing aspect of this studies, as well as many other papers discussed herein, relates to investigation of DES effect on catalyst quantum yields changes. Conclusions on this behavior as well as its reasons should be further explored in context of DES usefulness for catalysts synthesis.

Depending on the pH of a solution, the catalyst chemically can affect the degradation rate through the changing of its charge surface, redox potential of active species, and properties of the target pollutant [120,121]. This phenomenon can also occur for DES-assisted catalysts. Ciğeroğlu et al. discussed the positive charge of ZnO/GO/DES and the negative charge of the cefixime (caused by the presence of two carboxylic acids and its p*K*a), which leads to an electrostatic interaction between the pollutant and catalyst [95]. Sometimes, the synthesis of a catalyst in DES medium boosts the reactions. Song et al. compared the zero charge point of Ti_3C_2 (<1), Ti_3C_2–HF/TiO_2 (traditional type; 3.2), and Ti_3C_2/TiO_2-80 (DES prepared by 80 mM $NaBF_4$; 5.76) for assessing the photocatalytic degradation of perfluorooctanoic acid [99]. The pH lower than the point of zero charge leads to a positive charge for each compound. When the pH of the solution is higher than 2.80 (the range of pH 2.8 to 5.76), perfluorooctanoic acid present as its deprotonated form ($C_{17}F_{15}COO^-$), causing strong adsorption between perfluorooctanoic acid and Ti_3C_2/TiO_2-80. Nevertheless, in some cases, the structure of DES causes an influential role in catalyst performance. For example, Taghavi et al. stated that the critical role of $ZnCl_2$ groups of the DES applied for synthesizing TiO_2–P25@TDI@DES on the photocatalytic activity by providing efficient Lewis acidic sites [92].

Similar to catalysts, pH variation affects the degradation effectiveness. Iqbal et al. tested the effect of pH (2.8–11.3) on flumequine's photocatalytic degradation rate [102]. The maximum yield was obtained at the pH of 6.8, while the rate was 43 and 35 % for the lowest and highest pH levels, respectively. According to the values related to point of zero charge and p*K*a (flumequine), the catalyst surface and pollutant had the same charge (both - positive charge at highly acidic pH and both negative at highly alkaline pH), initiating electrostatic repulsion reaction, and led to the degradation performance reduction. They also observed the same trend during the sulfamethaxazole degradation [103]. Further, it was proved that the presence of external Brønsted acid could improve the photochemical yield [122,123]. Taghavi et al. achieved a maximum of 78% degradation rate (4 × 3 W blue LED lamps, emitting light >420 nm) for primary benzyl alcohols, when they used sodium nitrate as the oxidant [92]. This limited rate attributed to insufficient concentration of H^+ for reducing nitrate. They obtained the 100% conversion after adding stoichiometric amount of the Brønsted acid, demonstrated their claim.

Scavengers usually are utilized for clarifying the major photocatalytic active species. Wu et al. used *p*-benzoquinone, ammonium oxalate, and isopropyl alcohol as $^{\bullet}O_2^-$, h^+, and $^{\bullet}OH$ scavengers, respectively [98]. They noticed an Rhodamine B (organic dye) degradation rate of 18%, 24%, and 98% for the corresponding quenchers, respectively, proving $^{\bullet}O_2^-$ and h^+ as the main active species. $^{\bullet}O_{2-}$ and h^+ are also known as the main quenchers when benzoquinone (BQ), silver nitrate ($AgNO_3$), and EDTA-2Na were added to the process in another work [97]. The group of Jaihindh et al. reported that h^+ and $^{\bullet}OH$ were the main species responsible for degradation [101]. Jaihindh and Fu [50] and Baby et al. [96] after following the same approach introduced h^+ and $^{\bullet}OH$ as considerable suppressing agents, respectively. It is interesting to note a gap that clearly determines the role of DES-assisted catalysts on the active species. Indeed, no study was focused specifically on the role of DES-assisted catalyst and the type of major photocatalytic active species. Wu et al. briefly discussed the diverse effect of valence band potential of CdS and CeO_2 on the formation of $^{\bullet}OH$ [98]. Nevertheless, just Iqbal et al. compared the suppressing action of several scavengers for quenching of e^-, h^+, and $^{\bullet}OH$ for DES- ceria and ceria catalysts. They reported same manned for both catalysts with dominant role of hydroxyl radicals [102].

Table 2
Operational parameters of AOPs catalyzed by DES-assisted catalysts.

Ref.	Catalyst name	Type of oxidant/AOP	Key radicals	Target pollutant	Operational Parameters						Activation method	Remarks on differences DES vs non-DES catalysts
					CoP[a] (ppm)	CD[b] (g L^{-1})	pH	Time (min)	Tem[c] (°C)	RE[d] (%)		
[92]	n-TiO2-P25@TDI@DES	NaNO3/PC	–	Benzyl alcohols	150,000	10	–	1200	RT	~75	4 × 3W blue LED	–
[35]	amorphous Fe NP	H_2O_2/PC-F	$O_{2\cdot}^{\bullet}$	RhB	25	1	–	30	RT	91	UV	–
[93]	nanosized anatase titania	PC	–	MO, reactive orange 16 and procion yellow H-E3G	20	0.45	–	60	RT	100	125 W UV	–
[94]	N/P co-doped TiO_2	PC + El	–	RhB and MB mixed solution of RhB and MB OTC	25 and 15 15 25	0.33	–	64	RT	100	300 W Xe	–
[95]	ZnOGO	PC	–	Cefixime trihydrate	20–50	0.3–0.7	4–10	60	40	80	4 × 15 W UVA	–
[96]	AFe_2O_4 (A = Mg, Zn and Mn)	H_2O_2/H-pF	e−, h+, •OH, $O_{2\cdot}^{\bullet}$ and •OOH	MB	25	1	1–13	120	RT	91 (MFM) 91 (ZnFM) > 99 (MnFM	4 × 8W fluorescent black light	–
[97]	CdS@CeO_2	PC	–	Tetracycline	50	0.05	–	60	RT	90	300 W Xe	–
[98]	$\|C_{10}H_{10}N_2\|$[GaF$(C_2O_4)_2$]	PC	O_2-• and h+	RhB	10	0.5	–	70	RT	99	300W Xe	–
[99]	Ti_3C_2/TiO_2–$NaBF_4$	PC	–	Perfluorooctanoic acid	20	0.2	–	1440	RT	100	UV	–
[100]	ZnO/NG	PC	•OH, O2-•	MB	100	1	–	90 (UV) 120 (visible)	RT	93	300 W UV 300 W Xe	–
[101]	BOC/BVO/g-CN	PC	h+, •OH	MO	20	0.2	–	210	50	96	35 W Xe	–
[102]	ceria NP	PC	•OH	Flumequine	2.5–20	0.05–0.5	3–11	120	RT	94	2 × 15W UV-C	–
[103]	nitrogen-doped (*N*-doped) Ceria nanoparticles	PC	•OH	Sulfamethaxazole	2.5–20	0.1–1	1–11	150	RT		300 W Xe	–
[38]	ε-manganese dioxide (ε-MnO_2)	H_2O_2/PC	–	RhB	20	0.73	–	120–480	RT	~96	20 W LED	–
[104]	α-Fe_2O_3 (hematite) nanoparticles.	PC	•OH, HO2-•	RhB	25	0.5	–	75	RT	55 and 47	150 W Xe	–
[105]	$BiVO_4$	PC	–	Cr(VI)	100	0.2	–	160	50	96	35 W Xe	–
[106]	Ag@AgCl	PC	O2-	Benzidine		–	–	70	RT	~98	300 W Xe	–
[107]	Ni–TiO_2 Composite	PC	–	MB	5	0–15	–	105	RT		UV	–
[108]	coral-like TiO_2 NP/ anatase and anatase-rutile TiO2	PC	–	MO	20	0.3	–	240	RT	98	150 W UV	–
[50]	BiOCl/ $BiVO_4$@AgNWs	PC	–	MB RhB	10	0.2	–	180	RT	98 96	35 W Xe	–
[86]	Mn_2O_3 nanoparticles	PC	–	Safranin-O	350	–	–	~75	RT			–
[41]	ZnO NPs	PC	–	MB	20	0.4	–	75	RT	~100	UV	–
[109]	TiO_2 NPs	PC	–	Orange II	20	1	–	360	RT	95.5 (UV) 59.8 (visible)	150 W UV and visible light	Compared to the commercial TiO2, two times higher removal efficiency was observed under

(*continued on next page*)

Table 2 (*continued*)

Ref.	Catalyst name	Type of oxidant/AOP	Key radicals	Target pollutant	Operational Parameters						Activation method	Remarks on differences DES vs non-DES catalysts
					CoP[a] (ppm)	CD[b] (g L^{-1})	pH	Time (min)	Tem[c] (°C)	RE[d] (%)		
[110]	ZnO nanosheets	PC	•OH	MB RhB	10	0.2 0.5	–	120	RT	0–100	UV	visible light illumination for the DES-assisted synthesized product. Presence of urea in the DES led to formation of zinc carbonate hydroxide, which decreased the photocatalytic efficiency.
[111]	ZnO	PC	•OH	MB	10	0.2	–	120	RT	~40–100	500 W UV	–
[112]	$BiVO_4$ microtubes	PC	–	RhB	10	2	–	300	RT	16–98	500 W Xe	–
[113]	titanomagnetite NP	H_2O_2/ peroxidase-like activity	•OH, HO_2-•, O_2-•	MB	10	0.5	6.5	120	RT	99.20	Fe	The k values achieved on the DES-assisted catalyst were one order of magnitude higher than those obtained in the aqueous solution.
[114]	cubic Iron oxide NP	H_2O_2/H-pF	•OH	RhB	10	–	–	180	RT	94.04	Fe + 6 × 8W UV	–
[115]	Fe_3O_4 magnetic NP	H_2O_2/ Fenton-like	•OH	RhB	10	0.5	5–9	120	25–70	99.80	Fe + thermal process	The removal efficiency of DES-assisted catalyst was 98%, and water-assisted catalyst showed 81% degradation efficiency.
[116]	nitrogen-doped biochar	PDS/Sulfate-based AOP	$^1O_2$	Tetracycline	20	0.1	3–9	150	RT	>92	biochar	The governed PDS activation pathway by the catalyst changed from reactive species-mediated oxidation to electron-shuttle mediated oxidation after DESs were utilized.

a: Concentration of the Pollutant	methylene blue	MB	Photocatalysis	PC	Room Temperature (25 °C)	RT
b: Catalyst dose	Rhodamine B	RhB	Electrolysis	El		
c: Temperature	methyl orange	MO	Heterogeneous Photo-Fenton	H-pF		
d: Removal efficiency	oxytetracycline dihydrate	OTC				

Conclusions

Catalysts synthesized in a DES environment showed higher activity in the AOPs compared to catalysts synthesized without DES. First of all, it is clear that the correct selection of DES affects the effect of catalyst efficiency improvements in AOPs. To date, it has not been possible to formulate general rules for DES selection. The most popular DESs that was used – with success – for catalysts synthesis include choline chloride based DESs with different HBD like urea, glycols (ED, DEG), sugars, organic acids (acetic acid, malonic acid, oxalic acid). In combination with ChCl, ionic HBDs like ferric chloride, HPF6, HBF4 also revealed usefulness. Up till now, contribution of very popular hydrophobic DESs (HDESs) was not reported.

Major DES contribution in the synthesis include the roles of, stabilizing/capping, structure-directing, template/hydrolyzing agent, etching agent/intercalator, latent supramolecular catalyst as well as obvious roles of solvent or electrolyte. Components of DESs can play a role of reductant or source of reagent for synthesis (for example oxalate ions source). DESs proved to significantly affect ("tune") catalyst morphology as well as photocatalytic properties (bad-gap regulation).

In overall materials such as metal oxides, MO complexes, MO-doped and MO-supported as well as inorganic-organic hybrids as well as carbo-catalysts were successfully obtained in DES-assisted synthesis. Effective modifications were obtained for popular photocatalytic materials such as TiO_2, ZnO, MnO_2, iron oxides, ceria oxide, cadmium sulfide (CdS) and bismuth based photocatalysts. Positive effects were also obtained for biochar modification.

Positive effects of DES-modified catalysts should be further studied based on normalized parameters for example the fluence. If the degradation effectiveness data are not normalized to the fluence, different applied light intensities may make the result incomparable. Secondly, further studies should address the aspects of DES effect on the change in the quantum yields, which can be helpful in revealing of DES role on improvement of catalyst performance. Currently, knowledge on this aspect is scarce.

The side effect of DES-based catalysts is not limited to the catalyst application. Through the synthesis process, specifically electrochemical processes, the toxic chemical compounds might be formed from DES components, questioning the green and safe properties of DES-assisted synthesis techniques. This aspects up-till now was not identified, as the authors didn't focus on this issue. It is already clear, that toxicity aspects of DESs and their effect on the environment already was overlooked in several DES applications [18, 124,125]. Undoubtedly, it is significantly important to select the right components for the preparation of DESs or choose the proper techniques in order to synthesize the catalysts. There are still huge gaps that obscure the DESs' roles and effect on the AOPs parameters. Moreover, there is no data on the recovery of DESs in the synthesis processes of catalysts applied in the AOPs, which at least has to be clear regarding the economic and green aspects of their application.

CRediT authorship contribution statement

Amir Mohammad Sheikh Asadi: Writing – review & editing, Writing – original draft, Visualization, Formal analysis, Data curation. **Łukasz Cichocki:** Data curation, Formal analysis, Writing – original draft, Writing – review & editing. **Ali Atamaleki:** Writing – original draft, Data curation. **Marjan Hashemi:** Writing – original draft, Data curation. **Holger Lutze:** Writing – review & editing. **Muhammad Imran:** Writing – review & editing. **Lingshuai Kong:** Writing – review & editing. **Chongqing Wang:** Writing – review & editing. **Grzegorz Boczkaj:** Writing – review & editing, Writing – original draft, Validation, Supervision, Project administration, Methodology, Conceptualization.

Declaration of competing interest

The authors declare that they have no known competing financial interests or personal relationships that could have appeared to influence the work reported in this paper.

Data availability

No data was used for the research described in the article.

Acknowledgments

The authors gratefully acknowledge the financial support from the National Science Centre, Warsaw, Poland – decision no. UMO-2018/30/E/ST8/00642.

References

[1] L. Wang, D. Luo, O. Hamdaoui, Y. Vasseghian, M. Momotko, G. Boczkaj, et al., Bibliometric analysis and literature review of ultrasound-assisted degradation of organic pollutants, Sci. Total Environ. (2023) 876.
[2] K. Fedorov, M. Plata-Gryl, J.A. Khan, G. Boczkaj, Ultrasound-assisted heterogeneous activation of persulfate and peroxymonosulfate by asphaltenes for the degradation of BTEX in water, J. Hazard Mater. 397 (2020) 122804.
[3] N.S. Shah, J. Iqbal, M. Sayed, A.A. Ghfar, J.A. Khan, Z.U.H. Khan, et al., Enhanced solar light photocatalytic performance of Fe-ZnO in the presence of H2O2, S2O82−, and HSO5− for degradation of chlorpyrifos from agricultural wastes: toxicities investigation, Chemosphere 287 (2022) 132331.
[4] K. Fedorov, X. Sun, G. Boczkaj, Combination of hydrodynamic cavitation and SR-AOPs for simultaneous degradation of BTEX in water, Chem. Eng. J. 417 (2021) 128081.

[5] S. Xiao, M. Cheng, H. Zhong, Z. Liu, Y. Liu, X. Yang, et al., Iron-mediated activation of persulfate and peroxymonosulfate in both homogeneous and heterogeneous ways: a review, Chem. Eng. J. 384 (2020) 123265.
[6] X. Ge, C.D. Gu, X.L. Wang, J.P. Tu, Deep eutectic solvents (DESs)-derived advanced functional materials for energy and environmental applications: challenges, opportunities, and future vision, J. Mater. Chem. A 5 (18) (2017) 8209–8229.
[7] H. Liu, X. Li, X. Zhang, F. Coulon, C. Wang, Harnessing the power of natural minerals: a comprehensive review of their application as heterogeneous catalysts in advanced oxidation processes for organic pollutant degradation, Chemosphere 337 (2023) 139404.
[8] L. Wang, D. Luo, J. Yang, C. Wang, Metal-organic frameworks-derived catalysts for contaminant degradation in persulfate-based advanced oxidation processes, J. Clean. Prod. 375 (2022) 134118.
[9] A.M. Sheikh Asadi, M. Malakootian, E. Kowsari, H. Alidadi, Ionic liquid-assisted sol-gel synthesis of Fe2O3-TiO2 for enhanced photocatalytic degradation of bisphenol a under UV illumination: modeling and optimization using response surface methodology, Optik 204 (2020) 164229.
[10] V.K. Landge, S.H. Sonawane, M. Sivakumar, S.S. Sonawane, G.U.B. Babu, G. Boczkaj, S-scheme heterojunction Bi2O3-ZnO/Bentonite clay composite with enhanced photocatalytic performance, Sustain. Energy Technol. Assessments 45 (2021) 9.
[11] A.M. Sheikh Asadi, M. Malakootian, Preparation and characterization of Fe/TiO2 in the presence of ionic liquid to optimize the photocatalytic degradation of acetaminophen using the response surface methodology, J. Mater. Sci. Mater. Electron. 30 (16) (2019) 14878–14889.
[12] A. Tsuda, N.V. Konduru, The role of natural processes and surface energy of inhaled engineered nanoparticles on aggregation and corona formation, NanoImpact 2 (2016) 38–44.
[13] M.J. Rodriguez-Alvarez, S.E. Garcia-Garrido, S. Perrone, J. García-Álvarez, V. Capriati, Deep eutectic solvents and heterogeneous catalysis with metallic nanoparticles: a powerful partnership in sustainable synthesis, Curr. Opin. Green Sustainable Chem. 39 (2023) 100723.
[14] J. Vakros, The influence of preparation method on the physicochemical characteristics and catalytic activity of Co/TiO2 catalysts, Catalysts 10 (1) (2020) 88.
[15] K. Bourikas, J. Vakros, C. Fountzoula, C. Kordulis, A. Lycourghiotis, Interface science for optimizing the size of oxidic nanoparticles in supported catalysts, Catal. Today 128 (3–4) (2007) 138–144.
[16] N. Kaur, V. Singh, Current status and future challenges in ionic liquids, functionalized ionic liquids and deep eutectic solvent-mediated synthesis of nanostructured TiO2: a review, New J. Chem. 41 (8) (2017) 2844–2868.
[17] A.P. Abbott, G. Capper, D.L. Davies, R.K. Rasheed, V. Tambyrajah, Novel solvent properties of choline chloride/urea mixtures, Chem. Commun. (1) (2003) 70–71.
[18] M. Marchel, H. Cieśliński, G. Boczkaj, Deep eutectic solvents microbial toxicity: current state of art and critical evaluation of testing methods, J. Hazard Mater. 425 (2022) 127963.
[19] S. Khandelwal, Y.K. Tailor, M. Kumar, Deep eutectic solvents (DESs) as eco-friendly and sustainable solvent/catalyst systems in organic transformations, J. Mol. Liq. 215 (2016) 345–386.
[20] I. Cichowska-Kopczyńska, B. Nowosielski, D. Warmińska, Deep eutectic solvents: properties and applications in CO2 separation, Molecules 28 (14) (2023) 5293.
[21] P. Savchenko, The nature of eutectics, Russ. J. Inorg. Chem. 4 (1959) 186–189.
[22] A.P. Abbott, D. Boothby, G. Capper, D.L. Davies, R.K. Rasheed, Deep eutectic solvents formed between choline chloride and carboxylic acids: versatile alternatives to ionic liquids, J. Am. Chem. Soc. 126 (29) (2004) 9142–9147.
[23] P. Anastas, N. Eghbali, Green chemistry: principles and practice, Chem. Soc. Rev. 39 (1) (2010) 301–312.
[24] K. Aruchamy, R.N. Maalige, M.M. Halanur, A. Mahto, R. Nagaraj, D. Kalpana, et al., Ultrafast synthesis of exfoliated manganese oxides in deep eutectic solvents for water purification and energy storage, Chem. Eng. J. 379 (2020) 122327.
[25] O.S. Hammond, S. Eslava, A.J. Smith, J. Zhang, K.J. Edler, Microwave-assisted deep eutectic-solvothermal preparation of iron oxide nanoparticles for photoelectrochemical solar water splitting, J. Mater. Chem. A 5 (31) (2017) 16189–16199.
[26] S. Datta, C. Jo, M. De Volder, L. Torrente-Murciano, Morphological control of nanostructured V2O5 by deep eutectic solvents, ACS Appl. Mater. Interfaces 12 (16) (2020) 18803–18812.
[27] A. Fernandes, P. Makoś, Z. Wang, G. Boczkaj, Synergistic effect of TiO2 photocatalytic advanced oxidation processes in the treatment of refinery effluents, Chem. Eng. J. 391 (2020) 123488.
[28] R.D.C. Soltani, M. Mashayekhi, M. Naderi, G. Boczkaj, S. Jorfi, M. Safari, Sonocatalytic degradation of tetracycline antibiotic using zinc oxide nanostructures loaded on nano-cellulose from waste straw as nanosonocatalyst, Ultrason. Sonochem. 55 (2019) 117–124.
[29] R.D.C. Soltani, Z. Miraftabi, M. Mahmoudi, S. Jorfi, G. Boczkaj, A. Khataee, Stone cutting industry waste-supported zinc oxide nanostructures for ultrasonic assisted decomposition of an anti-inflammatory non-steroidal pharmaceutical compound, Ultrason. Sonochem. 58 (2019) 104669.
[30] K. Fedorov, K. Dinesh, X. Sun, R. Darvishi Cheshmeh Soltani, Z. Wang, S. Sonawane, et al., Synergistic effects of hybrid advanced oxidation processes (AOPs) based on hydrodynamic cavitation phenomenon – a review, Chem. Eng. J. 432 (2022) 134191.
[31] G. Boczkaj, A. Fernandes, Wastewater treatment by means of advanced oxidation processes at basic pH conditions: a review, Chem. Eng. J. 320 (2017) 608–633.
[32] J.N. Baby, C. Lavanya, S.F. Wang, B. Sriram, A. Anantharaman, M. George, Sustainable synthesis of AFe2O4(A = Mg, Zn, Mn) catalysts: comparing the photooxidative and electrochemical properties towards organic dyes detection and degradation, New J. Chem. 45 (22) (2021) 10049–10056.
[33] J. Xu, M. Li, J.H. Qiu, X.F. Zhang, Y. Feng, J.F. Yao, PEGylated deep eutectic solvent-assisted synthesis of CdS@CeO2 composites with enhanced visible light photocatalytic ability, Chem. Eng. J. 383 (2020) 9.
[34] S.J. Ye, W.P. Xiong, J. Liang, H.L. Yang, H.P. Wu, C.Y. Zhou, et al., Refined regulation and nitrogen doping of biochar derived from ramie fiber by deep eutectic solvents (DESs) for catalytic persulfate activation toward non-radical organics degradation and disinfection, J. Colloid Interface Sci. 601 (2021) 544–555.
[35] V. Swathi Pon Sakthi Sri, A. Manikandan, M. Mathankumar, R. Tamizhselvi, M. George, K. Murugaiah, et al., Unveiling the photosensitive and magnetic properties of amorphous iron nanoparticles with its application towards decontamination of water and cancer treatment, J. Mater. Res. Technol. 15 (2021) 99–118.
[36] S. Sandhu, N. Kumar, V.P. Singh, V. Singh, Synthesis of reactive faceted nanosized titania with enhanced photocatalytic performance under fluorine free conditions using deep eutectic solvent, Vacuum 184 (2021) 9.
[37] J. Iqbal, N.S. Shah, M. Sayed, N. Muhammad, S.U. Rehman, J.A. Khan, et al., Deep eutectic solvent-mediated synthesis of ceria nanoparticles with the enhanced yield for photocatalytic degradation of flumequine under UV-C, J. Water Process Eng. 33 (2020).
[38] X. Lai, Y. Cheng, C. Han, G. Luo, Synthesis of ε-MnO2 in deep eutectic solvent for visible-light-driven photocatalytic activity, Mater. Res. Innovat. 23 (5) (2019) 305–309.
[39] M. Karimi, M.B. Lejbini, V. Jahangir, A.S. Jam, S. Mohammadzadeh, Amorphous and nanocrystalline hematite photocatalysts synthesized in ferric chloride-choline chloride acting as a green and reactive synthesis, Optik 181 (2019) 816–822.
[40] S.K. Shahi, N. Kaur, S. Sandhu, J.S. Shahi, V. Singh, Influences of a new templating agent on the synthesis of coral-like TiO2 nanoparticles and their photocatalytic activity, J. Sci. 2 (3) (2017) 347–353.
[41] T. Cun, C. Dong, Q. Huang, Ionothermal precipitation of highly dispersive ZnO nanoparticles with improved photocatalytic performance, Appl. Surf. Sci. 384 (2016) 73–82.
[42] L. Anicai, A. Petica, D. Patroi, V. Marinescu, P. Prioteasa, S. Costovici, Electrochemical synthesis of nanosized TiO2 nanopowder involving choline chloride based ionic liquids, Materials Science and Engineering B-Advanced Functional Solid-State Materials 199 (2015) 87–95.
[43] J.Y. Dong, C.H. Lin, Y.J. Hsu, S.Y. Lu, D.S.H. Wong, Single-crystalline mesoporous ZnO nanosheets prepared with a green antisolvent method exhibiting excellent photocatalytic efficiencies, CrystEngComm 14 (14) (2012) 4732–4737.
[44] J.Y. Dong, W.H. Lin, Y.J. Hsu, D.S.H. Wong, S.Y. Lu, Ultrafast formation of ZnO mesocrystals with excellent photocatalytic activities by a facile Tris-assisted antisolvent process, CrystEngComm 13 (20) (2011) 6218–6222.

[45] V. Sri, J. Taj, M. George, Facile synthesis of magnetite nanocubes using deep eutectic solvent: an insight to anticancer and photo-Fenton efficacy, Surface. Interfac. 20 (2020) 10.
[46] F. Chen, S. Xie, X. Huang, X. Qiu, Ionothermal synthesis of Fe 3 O 4 magnetic nanoparticles as efficient heterogeneous Fenton-like catalysts for degradation of organic pollutants with H 2 O 2, J. Hazard Mater. 322 (2017) 152–162.
[47] H. Song, Y. Wang, Z. Ling, D. Zu, Z. Li, Y. Shen, et al., Enhanced Photocatalytic Degradation of Perfluorooctanoic Acid by Ti3C2 MXene-Derived Heterojunction Photocatalyst: Application of Intercalation Strategy in DESs, Science of the Total Environment, 2020, p. 746.
[48] D.P. Jaihindh, A. Manikandan, Y.L. Chueh, Y.P. Fu, Deep eutectic solvent-assisted synthesis of ternary heterojunctions for the oxygen evolution reaction and photocatalysis, ChemSusChem 13 (10) (2020) 2726–2738.
[49] D.P. Jaihindh, B. Thirumalraj, S.M. Chen, P. Balasubramanian, Y.P. Fu, Facile synthesis of hierarchically nanostructured bismuth vanadate: an efficient photocatalyst for degradation and detection of hexavalent chromium, J. Hazard Mater. 367 (2019) 647–657.
[50] D.P. Jaihindh, Y.-P. Fu, Facile synthesis of deep eutectic solvent assisted BiOCl/BiVO4@AgNWs plasmonic photocatalysts under visible light enhanced catalytic performance, Catal. Today 297 (2017) 246–254.
[51] W. Liu, Y.Q. Yu, L.X. Cao, G. Su, L. Zhang, Y.G. Wang, Spindle like BiVO4 microtubes: synthesis in deep eutectic solvent and photocatalytic properties, Chin. J. Inorg. Chem. 26 (3) (2010) 379–384.
[52] W. Liu, Y.Q. Yu, L.X. Cao, G. Su, X.Y. Liu, L. Zhang, et al., Synthesis of monoclinic structured BiVO4 spindly microtubes in deep eutectic solvent and their application for dye degradation, J. Hazard Mater. 181 (1–3) (2010) 1102–1108.
[53] H.Y. Jia, M. Dong, Z.Y. Yuan, J.W. Chen, Z.D. Gong, J.A. Shao, Deep eutectic solvent electrolysis for preparing N and P co-doped titanium dioxide for rapid photodegradation of dyestuff and antibiotic, Ceram. Int. 47 (16) (2021) 23249–23258.
[54] J. Iqbal, N.S. Shah, M. Sayed, J. Ali Khan, N. Muhammad, Z.U.H. Khan, et al., Synthesis of nitrogen-doped Ceria nanoparticles in deep eutectic solvent for the degradation of sulfamethaxazole under solar irradiation and additional antibacterial activities, Chem. Eng. J. (2020) 394.
[55] F.I. Danilov, A.A. Kityk, D.A. Shaiderov, D.A. Bogdanov, S.A. Korniy, V.S. Protsenko, Electrodeposition of Ni-TiO2 composite coatings using electrolyte based on a deep eutectic solvent, Surf. Eng. Appl. Electrochem. 55 (2) (2019) 138–149.
[56] Z. Cigeroglu, S. Sahin, E.S. Kazan, One-pot green preparation of deep eutectic solvent-assisted ZnO/GO nanocomposite for cefixime trihydrate photocatalytic degradation under UV-A irradiation, Biomass Convers Biorefinery (2021) 14.
[57] X. Jin, Z.J. Ma, G.R. Liu, D.W. Hu, C.F. Song, Q. Huang, In-situ ionothermal precipitation of well-dispersed ZnO nanoparticles onto 2-dimension neat graphene sheets with excellent photocatalytic activity, J. Environ. Chem. Eng. 8 (4) (2020) 9.
[58] J.H. Ge, Y.C. Chen, J. Xu, Y.J. Liu, L. Zhang, F.G. Zha, Fabrication of Ag@AgCl with enhanced plasmonic photocatalysis performance via a deep eutectic solvent, Aust. J. Chem. 72 (3) (2019) 200–205.
[59] S. Taghavi, A. Amoozadeh, F. Nemati, The first report of deep eutectic solvent (DES) nano-photocatalyst (n-TiO2-P25@TDI@DES(urea:ZnCl2)) and its application on selective oxidation of benzyl alcohols to benzaldehydes, J. Chem. Technol. Biotechnol. 96 (2) (2021) 384–393.
[60] J.B. Wu, L.Q. Lou, H.Y. Sun, C.Y. Tao, T. Li, Z.P. Wang, et al., Photochromic inorganic-organic complex derived from low-cost deep eutectic solvents with tunable photocurrent responses and photocatalytic properties, CrystEngComm 22 (6) (2020) 1078–1085.
[61] Y. Sun, S.A. Cheng, Z.Z. Mao, Z.F. Lin, X.R. Ren, Z. Yu, High electrochemical activity of a Ti/SnO2-Sb electrode electrodeposited using deep eutectic solvent, Chemosphere 239 (2020) 7.
[62] C.J. Clarke, W.C. Tu, O. Levers, A. Brohl, J.P. Hallett, Green and sustainable solvents in chemical processes, Chem. Rev. 118 (2) (2018) 747–800.
[63] M. Karimi, M. Rastegar Ramsheh, S. Mohammad Ahmadi, M. Reza Madani, One-step and low-temperature synthesis of monetite nanoparticles in an all-in-one system (reactant, solvent, and template) based on calcium chloride-choline chloride deep eutectic medium, Ceram. Int. 43 (2) (2017) 2046–2050.
[64] S. Chaturvedi, P.N. Dave, N.K. Shah, Applications of nano-catalyst in new era, J. Saudi Chem. Soc. 16 (3) (2012) 307–325.
[65] S. Smeets, L.B. McCusker, Location of organic structure-directing agents in zeolites using diffraction techniques, in: L. Gómez-Hortigüela (Ed.), Insights into the Chemistry of Organic Structure-Directing Agents in the Synthesis of Zeolitic Materials, Springer International Publishing, Cham, 2018, pp. 43–73.
[66] C. Paris, M. Moliner, Role of supramolecular chemistry during templating phenomenon in zeolite synthesis, in: L. Gómez-Hortigüela (Ed.), Insights into the Chemistry of Organic Structure-Directing Agents in the Synthesis of Zeolitic Materials, Springer International Publishing, Cham, 2018, pp. 139–177.
[67] J.W. Steed, J.L. Atwood, Supramolecular Chemistry, 2nd,, John Wiley & Sons, 2009.
[68] M. Abbas, B. Parvatheeswara Rao, S.M. Naga, M. Takahashi, C. Kim, Synthesis of high magnetization hydrophilic magnetite (Fe3O4) nanoparticles in single reaction—surfactantless polyol process, Ceram. Int. 39 (7) (2013) 7605–7611.
[69] T.P. Vaid, S.P. Kelley, R.D. Rogers, Structure-directing effects of ionic liquids in the ionothermal synthesis of metal–organic frameworks, IUCrJ 4 (4) (2017) 380–392.
[70] S.M. Ghoreishi, Facile synthesis and characterization of CaWO4 nanoparticles using a new Schiff base as capping agent: enhanced photocatalytic degradation of methyl orange, J. Mater. Sci. Mater. Electron. 28 (19) (2017) 14833–14838.
[71] O.S. Hammond, D.T. Bowron, K.J. Edler, The effect of water upon deep eutectic solvent nanostructure: an unusual transition from ionic mixture to aqueous solution, Angew. Chem. Int. Ed. 56 (33) (2017) 9782–9785.
[72] Ł. Cichocki, D. Warmińska, J. Łuczak, A. Przyjazny, G. Boczkaj, New simple and robust method for determination of polarity of deep eutectic solvents (DESs) by means of contact angle measurement, Molecules 27 (13) (2022) 4198.
[73] A. Gutiérrez-Hernández, A. Richaud, L. Chacón-García, C.J. Cortés-García, F. Méndez, C.A. Contreras-Celedón, Deep eutectic solvent choline chloride/p-toluenesulfonic acid and water favor the enthalpy-driven binding of arylamines to maleimide in aza-michael addition, J. Org. Chem. 86 (1) (2021) 223–234.
[74] C.L. Boldrini, A.F. Quivelli, N. Manfredi, V. Capriati, A. Abbotto, Deep Eutectic solvents in solar energy technologies, Molecules 27 (3) (2022) 709.
[75] C.L. Boldrini, A.F. Quivelli, F.M. Perna, P. Biagini, V. Capriati, A. Abbotto, et al., Top-ranked Efficiency under Indoor Light of DSSCs Enabled by Iodide-Based DES-like Solvent Electrolyte, Sustainable Energy & Fuels, 2024.
[76] K. Haerens, E. Matthijs, K. Binnemans, B. Van der Bruggen, Electrochemical decomposition of choline chloride based ionic liquid analogues, Green Chem. 11 (9) (2009) 1357–1365.
[77] M. Marchel, H. Cieśliński, G. Boczkaj, Thermal instability of choline chloride-based deep eutectic solvents and its influence on their Toxicity—Important limitations of DESs as sustainable materials, Ind. Eng. Chem. Res. 61 (30) (2022) 11288–11300.
[78] A.P. Abbott, Deep eutectic solvents and their application in electrochemistry, Curr. Opin. Green Sustainable Chem. 36 (2022) 100649.
[79] L. Wang, H. Jiang, H. Wang, P.L. Show, A. Ivanets, D. Luo, et al., MXenes as heterogeneous Fenton-like catalysts for removal of organic pollutants: a review, J. Environ. Chem. Eng. 10 (6) (2022) 108954.
[80] B.A. Samejo, K. Sheikh, S. Samejo, F.A. Janjhi, N. Memon, R. Castro-Muñoz, et al., MXene-based composites for capacitive deionization–The advantages, progress, and their role in desalination-A review, Water Resour. Ind. (2023) 100230.
[81] A. Srivastava, A. Verma, Y.K. Prajapati, Chapter 4 - effect of 2D, TMD, perovskite, and 2D transition metal carbide/nitride materials on performance parameters of SPR biosensor, in: C.M. Hussain, S.K. Kailasa (Eds.), Handbook of Nanomaterials for Sensing Applications, Elsevier, 2021, pp. 57–90.
[82] Y. Li, X. Deng, J. Tian, Z. Liang, H. Cui, Ti3C2 MXene-derived Ti3C2/TiO2 nanoflowers for noble-metal-free photocatalytic overall water splitting, Appl. Mater. Today 13 (2018) 217–227.
[83] P. Szuromi, Watching metal nanoparticle exsolution, Science 366 (834) (2019).
[84] M. Ghidiu, M.R. Lukatskaya, M.-Q. Zhao, Y. Gogotsi, M.W. Barsoum, Conductive two-dimensional titanium carbide 'clay' with high volumetric capacitance, Nature 516 (7529) (2014) 78–81.
[85] J. Halim, S. Kota, M.R. Lukatskaya, M. Naguib, M.-Q. Zhao, E.J. Moon, et al., Synthesis and characterization of 2D molybdenum carbide (MXene), Adv. Funct. Mater. 26 (18) (2016) 3118–3127.
[86] H.S. Devi, T.D. Singh, Synthesis of Mn2O3 nanoparticles using choline chloride-ethylene glycol deep eutectic solvent: a green solvent, Integrated Ferroelectrics Int. J. 185 (1) (2017) 82–89.

[87] S.J. Bryant, A.J. Christofferson, T.L. Greaves, C.F. McConville, G. Bryant, A. Elbourne, Bulk and interfacial nanostructure and properties in deep eutectic solvents: current perspectives and future directions, J. Colloid Interface Sci. 608 (2022) 2430–2454.
[88] X. Tan, W. Zhao, T. Mu, Controllable exfoliation of natural silk fibers into nanofibrils by protein denaturant deep eutectic solvent: nanofibrous strategy for multifunctional membranes, Green Chem. 20 (15) (2018) 3625–3633.
[89] R. Castro-Muñoz, Ł. Cichocki, M. Plata-Gryl, G. Boczkaj, F. Galiano, Performance tuning of chitosan-based membranes by protonated 2-Pyrrolidone-5-carboxylic acid-sulfolane DES for effective water/ethanol separation by pervaporation, Chem. Eng. Res. Des. 191 (2023) 401–413.
[90] M. Thommes, K. Kaneko, A.V. Neimark, J.P. Olivier, F. Rodriguez-Reinoso, J. Rouquerol, et al., Physisorption of gases, with special reference to the evaluation of surface area and pore size distribution (IUPAC Technical Report), Pure Appl. Chem. 87 (9–10) (2015) 1051–1069.
[91] C. Xiao, B.-A. Lu, P. Xue, N. Tian, Z.-Y. Zhou, X. Lin, et al., High-index-facet- and high-surface-energy nanocrystals of metals and metal oxides as highly efficient catalysts, Joule 4 (12) (2020) 2562–2598.
[92] S. Taghavi, A. Amoozadeh, F. Nemati, The first report of deep eutectic solvent (DES) nano-photocatalyst (n-TiO2-P25@TDI@DES (urea: ZnCl2)) and its application on selective oxidation of benzyl alcohols to benzaldehydes 96 (2) (2021) 384–393.
[93] S. Sandhu, N. Kumar, V.P. Singh, V. Singh, Synthesis of reactive faceted nanosized titania with enhanced photocatalytic performance under fluorine free conditions using deep eutectic solvent, Vacuum 184 (2021) 109896.
[94] H. Jia, M. Dong, Z. Yuan, J. Chen, Z. Gong, J. Shao, Deep eutectic solvent electrolysis for preparing N and P co-doped titanium dioxide for rapid photodegradation of dyestuff and antibiotic, Ceram. Int. 47 (16) (2021) 23249–23258.
[95] Z. Ciğeroğlu, S. Şahin, E.S. Kazan, One-pot Green Preparation of Deep Eutectic Solvent-Assisted ZnO/GO Nanocomposite for Cefixime Trihydrate Photocatalytic Degradation under UV-A Irradiation, Biomass Convers Biorefinery, 2021.
[96] J.N. Baby, C. Lavanya, S.-F. Wang, B. Sriram, A. Anantharaman, M. George, Sustainable synthesis of AFe2O4 (A = Mg, Zn, Mn) catalysts: comparing the photooxidative and electrochemical properties towards organic dyes detection and degradation, New J. Chem. 45 (22) (2021) 10049–10056.
[97] J. Xu, M. Li, J. Qiu, X.-F. Zhang, Y. Feng, J. Yao, PEGylated deep eutectic solvent-assisted synthesis of CdS@CeO2 composites with enhanced visible light photocatalytic ability, Chem. Eng. J. 383 (2020) 123135.
[98] J. Wu, L. Lou, H. Sun, C. Tao, T. Li, Z. Wang, et al., Photochromic inorganic–organic complex derived from low-cost deep eutectic solvents with tunable photocurrent responses and photocatalytic properties, CrystEngComm 22 (6) (2020) 1078–1085.
[99] H. Song, Y. Wang, Z. Ling, D. Zu, Z. Li, Y. Shen, et al., Enhanced photocatalytic degradation of perfluorooctanoic acid by Ti3C2 MXene-derived heterojunction photocatalyst: application of intercalation strategy in DESs, Sci. Total Environ. 746 (2020) 141009.
[100] X. Jin, Z. Ma, G. Liu, D. Hu, C. Song, Q. Huang, In-situ ionothermal precipitation of well-dispersed ZnO nanoparticles onto 2-dimension neat graphene sheets with excellent photocatalytic activity, J. Environ. Chem. Eng. 8 (4) (2020) 104030.
[101] D.P. Jaihindh, A. Manikandan, Y.-L. Chueh, Y.-P. Fu, Deep eutectic solvent-assisted synthesis of ternary heterojunctions for the oxygen evolution reaction and photocatalysis 13 (10) (2020) 2726–2738.
[102] J. Iqbal, N.S. Shah, M. Sayed, N. Muhammad, S-u Rehman, J.A. Khan, et al., Deep eutectic solvent-mediated synthesis of ceria nanoparticles with the enhanced yield for photocatalytic degradation of flumequine under UV-C, J. Water Process Eng. 33 (2020) 101012.
[103] J. Iqbal, N.S. Shah, M. Sayed, J. Ali Khan, N. Muhammad, Z.U.H. Khan, et al., Synthesis of nitrogen-doped Ceria nanoparticles in deep eutectic solvent for the degradation of sulfamethaxazole under solar irradiation and additional antibacterial activities, Chem. Eng. J. 394 (2020) 124869.
[104] M. Karimi, M.B. Lejbini, V. Jahangir, A.S. Jam, S.M. Asl, Amorphous and nanocrystalline hematite photocatalysts synthesized in ferric chloride-choline chloride acting as a green and reactive synthesis medium, Optik 181 (2019) 816–822.
[105] D.P. Jaihindh, B. Thirumalraj, S.-M. Chen, P. Balasubramanian, Y.-P. Fu, Facile synthesis of hierarchically nanostructured bismuth vanadate: an efficient photocatalyst for degradation and detection of hexavalent chromium, J. Hazard Mater. 367 (2019) 647–657.
[106] J. Ge, Y. Chen, J. Xu, Y. Liu, L. Zhang, F. Zha, Fabrication of Ag@AgCl with enhanced plasmonic photocatalysis performance via a deep eutectic solvent, Aust. J. Chem. 72 (3) (2019) 200–205.
[107] F.I. Danilov, A.A. Kityk, D.A. Shaiderov, D.A. Bogdanov, S.A. Korniy, V.S. Protsenko, Electrodeposition of Ni–TiO2 composite coatings using electrolyte based on a deep eutectic solvent, Surf. Eng. Appl. Electrochem. 55 (2) (2019) 138–149.
[108] S.K. Shahi, N. Kaur, S. Sandhu, J.S. Shahi, V. Singh, Influences of a new templating agent on the synthesis of coral-like TiO2 nanoparticles and their photocatalytic activity, J. Sci.: Advanced Materials and Devices 2 (3) (2017) 347–353.
[109] L. Anicai, A. Petica, D. Patroi, V. Marinescu, P. Prioteasa, S. Costovici, Electrochemical synthesis of nanosized TiO2 nanopowder involving choline chloride based ionic liquids, Mater. Sci. Eng., B 199 (2015) 87–95.
[110] J.-Y. Dong, C.-H. Lin, Y.-J. Hsu, S.-Y. Lu, D.S.-H. Wong, Single-crystalline mesoporous ZnO nanosheets prepared with a green antisolvent method exhibiting excellent photocatalytic efficiencies, CrystEngComm 14 (14) (2012) 4732–4737.
[111] J.-Y. Dong, W.-H. Lin, Y.-J. Hsu, D.S.-H. Wong, S.-Y. Lu, Ultrafast formation of ZnO mesocrystals with excellent photocatalytic activities by a facile Tris-assisted antisolvent process, CrystEngComm 13 (20) (2011) 6218–6222.
[112] W. Liu, Y. Yu, L. Cao, G. Su, X. Liu, L. Zhang, et al., Synthesis of monoclinic structured BiVO4 spindly microtubes in deep eutectic solvent and their application for dye degradation, J. Hazard Mater. 181 (1) (2010) 1102–1108.
[113] J. Zhang, Z. Wang, R. Chen, F. Chen, New soft chemistry route to titanomagnetite magnetic nanoparticles with enhanced peroxidase-like activity, Powder Technol. 373 (2020) 39–45.
[114] S.P. Sakthi Sri, J. Taj, M. George, Facile synthesis of magnetite nanocubes using deep eutectic solvent: an insight to anticancer and photo-Fenton efficacy, Surface. Interfac. 20 (2020) 100609.
[115] F. Chen, S. Xie, X. Huang, X. Qiu, Ionothermal synthesis of Fe3O4 magnetic nanoparticles as efficient heterogeneous Fenton-like catalysts for degradation of organic pollutants with H2O2, J. Hazard Mater. 322 (2017) 152–162.
[116] S. Ye, W. Xiong, J. Liang, H. Yang, H. Wu, C. Zhou, et al., Refined regulation and nitrogen doping of biochar derived from ramie fiber by deep eutectic solvents (DESs) for catalytic persulfate activation toward non-radical organics degradation and disinfection, J. Colloid Interface Sci. 601 (2021) 544–555.
[117] A. Yazdanbakhsh, A. Eslami, F. Mahdipour, F. Ghanbari, S.M. Ghasemi, A. Atamaleki, et al., Dye degradation in aqueous solution by dithionite/UV-C advanced reduction process (ARP): kinetic study, dechlorination, degradation pathway and mechanism, J. Photochem. Photobiol. Chem. 407 (2021) 112995.
[118] H. Derikvandi, A. Nezamzadeh-Ejhieh, An effective wastewater treatment based on sunlight photodegradation by SnS2–ZnS/clinoptilolite composite, Solid State Sci. 101 (2020) 106127.
[119] Ł. Cichocki, L. Kong, C. Wang, A. Przyjazny, G. Boczkaj, First highly effective non-catalytic nitrobenzene reduction in UV/dithionite system with aniline production–Advanced reduction process (ARP) approach, Chem. Eng. J. 479 (2024) 147878.
[120] R.D. Chekuri, S.R. Tirukkovalluri, Synthesis of cobalt doped titania nano material assisted by gemini surfactant : characterization and application in degradation of Acid Red under visible light irradiation 24 (1) (2017) 183–195.
[121] P. Karimi, M. Malakootian, Optimization of photocatalytic degradation of naproxen from aqueous solutions with UV/ZnO process: response Surface Methodology (RSM), GLOBAL NEST JOURNAL 22 (3) (2020) 369–380.
[122] Q. Wang, M. Zhang, C. Chen, W. Ma, J. Zhao, Photocatalytic aerobic oxidation of alcohols on TiO2: the acceleration effect of a brønsted acid 49 (43) (2010) 7976–7979.
[123] D. Kozlov, D. Bavykin, E. Savinov, Effect of the acidity of TiO2 surface on its photocatalytic activity in acetone gas-phase oxidation, Catal. Lett. 86 (4) (2003) 169–172.
[124] M. Marchel, M.P. Rayaroth, C. Wang, L. Kong, J.A. Khan, G. Boczkaj, Hydrophobic (deep) eutectic solvents (HDESs) as extractants for removal of pollutants from water and wastewater – a review, Chem. Eng. J. (2023) 144971.
[125] F.A. Janjhi, R. Castro-Muñoz, G. Boczkaj, Deep eutectic solvents – ideal solution for clean air or hidden danger? Sep. Purif. Technol. 314 (2023) 123590.